Development and Testing of the LOVES Spectrograph

Petter Thorén

Lund Observatory
Lund University

2016-EXA104

Degree project of 60 higher education credits (for a degree of Master)
June 2016

Supervisors: Sven Huldt and Hampus Nilsson

Lund Observatory
Box 43
SE-221 00 Lund
Sweden

Abstract

In this report we present the testing and development made using the Lund Observatory Vacuum Echelle Spectrograph (LOVES) during the last few years. Hardware development includes an assembly from base components due to relocation and necessary calibrations of the optics. Software development includes the making of a basic image processing pipeline for the instrument. The testing of LOVES wavelength determination capabilities has been done by determining the wavelengths of a CCD exposure in the wavelength range between 2170-2570Å using secondary iron reference lines. A total of 459 line wavelengths have been measured. Comparing these lines to references leads to the conclusion that LOVES is capable of making good wavelength measurements but more work is still needed for it to become a good scientific instrument.

Acknowledgements

First, I would like to thank my supervisors, Sven Huldt and Hampus Nilsson for everything I learned during my master's work. Not all of it was physics, but it was all valuable. Henrik Hartman and the rest of the atomic physics group should also have thanks for their contributions to the thesis.

Second, I want to all my friends and colleagues at astro for all the time we spent together both inside and outside the department. Special thanks to my long-time officemates: Tryggvi, Ryan and Tim for making the sometimes slow days go by faster. Now at least half of us are finished! More people to thank are Daniel M for teaching me to use the telescopes and for many good observing nights and Kalle for always being there to have excellent discussions with. There are many amazing people I should also mention here; Georgi, Michiel, Chiara, Bert, Alexey, Asli, Mohsen, Matt and all the amazing people of the Gastronomy trip that I probably missed.

Finally, I should thank my family for not giving up on me when I spent just a little bit more time than planned on my degree. My Mother and Father, brother and sister and not least both my pairs of grandparents. Tack för att ni aldrig någonsin tyckte att jag skulle lägga av.

Contents

Populärvetenskaplig sammanfattning

Lunds Observatoriums Vakuum-Echelle Spektrograf (LOVES) är en spektrograf byggd för att studera ultraviolett ljus i våglängdsregionen 1000-2000Å. Ultraviolett (UV) ljus i denna våglängdsregion absorberas i luft varför LOVES är konstruerad inuti en 2,5m lång evakuerad tank. LOVES är i dagsläget inte ett helt fullbordat vetenskapligt instrument. Detta projekt har haft som mål att utveckla och testa LOVES förmåga att bestämma våglängder.

UV-ljus är en intressant våglängdsregion av flera anledningar. Flera vanliga grundämnen, t.ex. kol och syre har sina resonanslinjer, d.v.s. sina mest grundläggande spektrallinjer, i det här området. Det är också ett tekniskt utmanande område att arbeta i vilket gör att många av spektrallinjerna i området fortfarande är relativt okända när det gäller atomspektroskopiska data.

I och med att LOVES inte är helt fullbordad så har det här projektet innehållit utveckling av själva instrumentet. LOVES har utvecklats både hårdvarumässigt och mjukvarumässigt. Rent hårdvarumässigt är LOVES ett komplett instrument idag efter att ha nedmonterats för att flyttas precis i början av projektet. Projektet har också innefattat utveckling av programvara för att hantera data från instrumentet och en grundläggande process för bildbehandling av bilder från LOVES kamera har utvecklats. M.h.a. denna nya process har LOVES förmåga att mäta våglängder också testats. Eftersom detta är ett av de första test som gjorts så testades våglängdsbestämningen inte i UV-området. Istället användes området 2000-3000Å eftersom det är lättare att arbeta och hitta referenslinjer i.

Chapter 1

Introduction

The Lund Observatory Vacuum Echelle Spectrograph (LOVES) is an instrument designed to obtain high-resolution spectra in the vacuum ultra-violet (UV) spectral region, specifically in the wavelength region 1000 to 2000Å. This region is at the time of writing rather poorly known in terms of spectroscopic data, e.g., oscillator strenghts and precise wavelengths (see e.g., Brandt et al. (1999)). More on this in section 1.1 below. For this reason LOVES was envisioned to be a complement to the UV FTS that is currently operational in Lund Observatory. This project is a part in making LOVES a useful science instrument. Specifically, the aim is to see if self-consistent wavelengths can be obtained using iron reference lines. Traditionally, noble gas lines are used as reference lines. However, in the wavelength region we are working in for this project there are very few such lines. With LOVES being an unfinished instrument, it is important to test its capabilities in various areas. Specifically, this project aims to show that LOVES, in is current state, can consistently reproduce a set of reference wavelengths without necessarily using in-order reference lines. Since this project represents an early test of LOVES' capabilities it looks at the significantly easier-to-work-in 2000-3000Å region rather than the UV proper. This region is easier to work in since it has a larger set of well-measured reference lines that the 1000-2000Å-region does not.

Thus, the two main goals of the project are: first to see if it is possible to develop a procedure that will give internally consistent wavelengths when supplied with good reference lines. Second, is to determine the wavelengths of unmeasured lines in the wavelength range 2000-3000Å.

This report is divided into six main parts: the first part is an introduction to the project and concepts that are needed to understand how the instrument works. Second is a technical description of LOVES, listing its systems and their specifications. The third section is intended as a sort of "user's manual" for LOVES, serving as both a recounting of the laboratory work this project contained and a guide for any future users of LOVES.

Fourth is a list of the software and hardware development that has been done for LOVES during the course of this project. Fifth is a description of the data reduction and wavelength determination process that allows the testing of LOVES' ability to determine self-consistent wavelengths. Sixth and finally is a short discussion section discussing the results of the project and what could be done in the future.

An Introduction to Gratings

LOVES is an echelle spectrograph which means that its main dispersive element is an echelle grating. In order to understand how LOVES works understanding the echelle is essential.

The basic concept of a grating is well known: it is a large number of evenly spaced slits that let light through. In the case of a reflection grating the slits are replaced with ruled or etched grooves on a mirror surface. In either case the grooves or slits act as a large amount of coherent light sources and the light that is transmitted or reflected by the grating forms a diffraction pattern. From here we will be discussing reflection gratings, since that is what LOVES uses, but much of theory is applicable to transmission gratings as well. The condition that light of a wavelength λ from all grooves of the grating will interfere constructively is known as the grating equation. (eq. 1.1).

$$m\lambda = d(\sin\alpha + \sin\beta) \tag{1.1}$$

Here α and β are the incident and exiting angles of the light, relative to the grating normal. β is considered to be positive if it is on the same side of the grating normal as α and negative otherwise. m is an integer, the so-called order number and d is the distance between the grooves. From eq. 1.1 follows that any given wavelength may be diffracted in multiple angles, one for each order number.

Modern gratings are often blazed (Thorne et al., 1999). This means that their grooves are given a sawtooth-shape in order to maximize the efficiency of the reflection in a certain direction. This is vital not least in the UV where reflectivity drops rapidly with decreasing wavelength. The sawtooth-shape of the grooves means that at some incident angle, depending on the angle of the grooves, there will be specular reflection[1] of the light. This means that there is a defined blaze wavelength for a conventional grating wherein its efficiency is maximised. If the angle of the sawtooth-step grooves relative to the surface of the grating is θ and α and β are the incident and exiting angles of the light relative to the normal of the grating as per fig. 1.1. We

[1]Specular reflection is when incident angle is equal to exiting angle, i.e. like in a plane mirror.

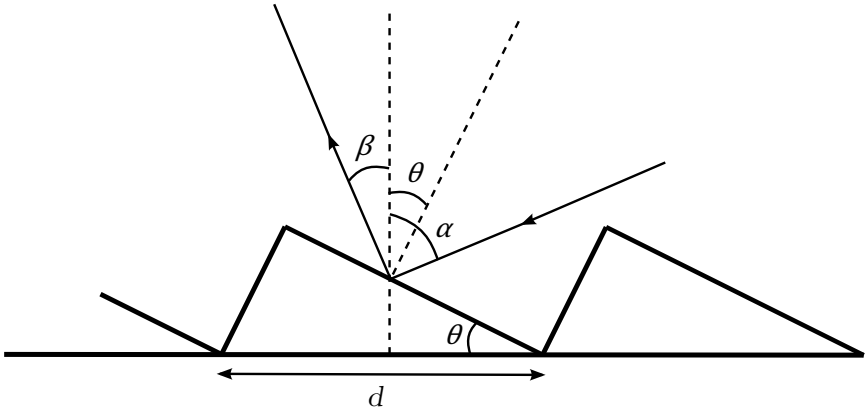

Figure 1.1: Illustration of a blazed grating. Adapted from similar illustration 12.25 in Thorne et al. (1999)

then get that (β is negative because it's on the opposite side of the normal relative to α)

$$\alpha - \theta = -\beta + \theta$$

$$2\theta = \alpha + \beta$$

It is then possible to use the grating equation, eq. 1.1 to determine the blaze wavelength.

$$m\lambda_{blaze} = 2d\mathrm{Sin}\theta\cos(\alpha - \theta).$$

Additionally, if we mount the grating such that the steps are perpendicular to the incident light in the so-called Littrow configuration we get that $\alpha = \beta = \theta$ and thus

$$m\lambda_{blaze} = 2d\sin\alpha = 2d\sin\theta. \tag{1.2}$$

The Littrow configuration is often used, especially for echelle spectrographs, since it simplifies the optics mountings and minimises optical aberration. (Thorne et al., 1999). An echelle grating is a special type of grating that has relatively large groove spacing. The reason for this is that for a spectrometer, resolving power can be expressed as

$$\mathcal{R} = W\frac{m}{d}. \tag{1.3}$$

Where W is the width of the grating, m is the order number and d is the size of the groove spacing (Thorne et al., 1999). Theoretically, it is possible to increase the resolving power by simply increasing the width of the grating. This is not feasible in reality, however, since the surface of the grating needs to be extremely homogeneous over the entire surface and maintaining such

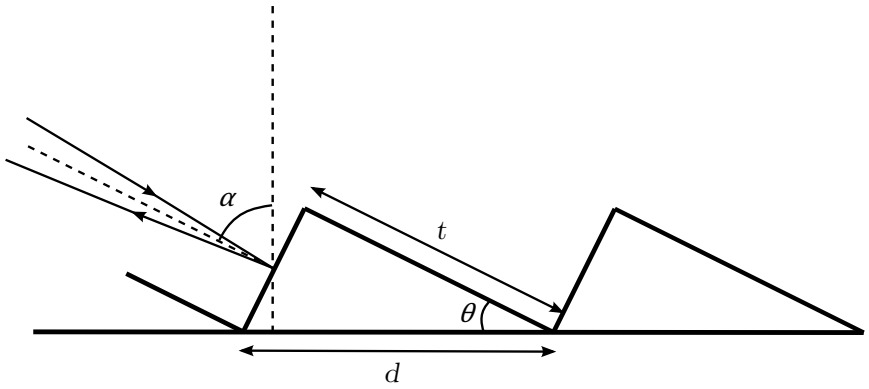

Figure 1.2: Illustration of an echelle grating. Note that the reflection is now in the short side of the sawtooth-shaped groove compared to fig. 1.1. Adapted from similar illustration 12.27 in Thorne et al. (1999)

accuracy over large surfaces is mechanically very difficult. This leaves us with the options of either having coarse grooves and looking at a high order or looking at a low order with fine grooves if we want to maintain high resolving power. The echelle grating is the former option.

Fig. 1.2 shows the equivalent of fig. 1.1 for an echelle grating. In the case of the echelle grating in LOVES the incident angle is related to the angle of the grooves as

$$\theta = 90^\circ - \alpha.$$

This means that for the echelle grating the blaze condition becomes

$$m\lambda_{blaze} = 2dsin\alpha = 2dcos\theta = 2t.$$

Cf. eq. 1.2. As shown above we must use high m to get good resolving power with an echelle grating. Often in the order of 100, which means that quite a large wavelength range can fit inside a handful of orders. This fact means that a blaze wavelength is usually not specified for an echelle grating; a blaze angle is used instead.

The high dispersion order that is used with an echelle grating means that the orders overlap significantly. To make it possible to look at individual orders some way to separate them is needed. This is the purpose of the order sorter grating (OSG) or more generally, the cross-disperser. The cross-disperser's disperses the light coming from the echelle grating in the direction perpendicular to the echelle's dispersion direction. This enables the separation of the echelle's tightly packed dispersion orders. The cross-disperser is usually a standard reflection grating, but can in theory be any sort of dispersive element.

The Vacuum Ultra-violet Region

The Vacuum UV region is defined by Edlén (1963) as "that part of the ultra-violet to which air is more or less opaque." This definition is then bounded at the upper end by the absorption of oxygen at about 1950Å and at the lower end by the point at which air again becomes transparent, at roughly 2Å . However, below 10Å there is a radical shift in observation technique due to light shifting into soft x-rays. It it therefore useful to to cut the defined region short at 10Å and extend the upper end to 2000Å for convenience sake, since neither of these are hard boundaries in reality. When discussing the 'UV region' below, this definition (10-2000Å) is the one we will use. Astute readers might note that the upper boundary here is 1000Å lower than the customary edge of the optical region in astronomy, at 3000Å. This is because the main absorber between 2000 and 3000Å is atmospheric ozone, which we do not have to worry about at sea level.

Due to the opaqueness of air it is necessary to work in either vacuum or some other gas to avoid absorption of the light one is trying to study. Vacuum works for the entire region and He is transparent down to 500Å. He-filled chambers are expensive to maintain and have today largely been replaced by vacuum chambers due to the much cheaper and more effective modern vacuum pumps. LOVES works with a vacuum pumping system that is detailed in section 2.2.

The Vacuum UV region has a few more challenges than absorption in air. Notably at below 1100Å LiF, the last solid to stay transparent becomes opaque. This means no windows can be used in the instrument, which complicates the connection of the light-source to the vacuum tank somewhat. Furthermore, there is a restriction on any gas pressure in the light source since high-pressure gas will absorb light at low wavelengths. LOVES is designed to operate mainly above this 1100Å limit where LiF is still transparent. However, it is possible to operate LOVES without a window since it gives better signal due to no absorption in the glass. More one this in section 3. Finally, below 1100Å mirrors rapidly lose reflectivity except at very high incident angles making more than one reflective optical component impractical because it leads to very large instrument sizes. (Edlén, 1963)

1.1 Project Motivation

Since the Ultra-violet is a technically challenging wavelength region to work in it is still relatively unknown in terms of spectroscopic data. Leckrone et al. (1999) and Brandt et al. (1999) is the end of a large effort to survey and catalogue astrophysically interesting spectroscopic data in the UV. The project used the Hubble space telescope to take spectra of chemically peculiar main-sequence stars, χ Lupi in particular, in order to catalogue the UV spectral region. Since this endeavour in the 1990's little systematic

catalogisation of the UV region has been carried out.

The UV is an interesting region for atomic physics since many elements, not least iron, has large parts of its spectrum in the region. Even though much of the UV astronomy in the world is somewhat stagnant today the Cosmic Origins Spectrograph on the Hubble Space Telescope is still in use. Furthermore, the FUSE satellite data is still being used (e.g., Richter et al. (2015)) for UV spectroscopy despite the satellite itself being decommissioned in 2007. Additionally, the UV is still important when determining, e.g., branching fractions for various elements. These are needed for calculating $\log gf$-values for spectral lines, even outside the UV, something that is in high demand today.

LOVES was originally conceived and constructed in the early 2000's as a complement to the existing vacuum Fourier transform spectrometer at Lund Observatory used to perform measurements for the χ Lupi pathfinder project. The need for accurate data in this region is still as large as it was when the instrument was designed and this project is a step on the way of getting LOVES in a state where it's possible to do science with.

The project itself is mainly a proof-of-concept to show that it is possible to use LOVES for doing useful science and that it is worth spending resources to streamline the measurement process. Specifically, we want to measure accurate wavelengths. To do this, we need a way to measure wavelengths in an arbitrary point in LOVES's available wavelength range. Preferably with as few external references as possible.

1.2 Original Aim and Motivation

Originally the aim of this project was different. However restoring LOVES to full functionality was always the first priority. When that turned out to be more time consuming than anticipated the ambition of using LOVES was changed. From the start the goal was to measure the wavelengths of the resonance lines of carbon and oxygen. The spectra of both OI and CI has less than 50% of the lines measured in the wavelength range 1000-2000 Åwhen looking at the NIST and Kurucz' on-line atomic spectra databases. When looking at the measured lines, a large majority of the data comes from spectral line lists published by the US National Bureau of Standards in the 1970's. Relevant publications are Moore (1976) for OI and Moore (1970) for CI. Both of these collect data from measurements done in the 1960's or earlier. This shows that there is a need to update these measurements and provide new ones where none exist.

Chapter 2

The Lund Observatory Vacuum Echelle Spectrograph

LOVES is an ultra-violet vacuum echelle spectrometer. As such, it is designed to accurately produce spectra in the ultra-violet region despite the instrumental challenges in doing so. Broadly speaking, LOVES consists of three systems: the vacuum system, the optics (including the detector) and the light source. The rest of this section is divided into three parts, each one describing one of the three systems.

LOVES was designed as an echelle spectrograph because it results in a comparatively high resolving power in a compact instrument. The reasons for this are discussed further in section 2.1 and are quantified in eq. 1.3 in the same section.

2.1 Optics

LOVES has three main optical elements and two other necessities. In this section we will talk briefly about the various elements in the order that they appear in the light-path. Furthermore, in this section, these elements will be accompanied by a number (n) that refers to the same number in figure2.1 and the accompanying table.

The first element is the entrance aperture (1). LOVES is capable of mounting various types of entrance apertures for differing needs. The standard aperture is circular with a diameter of 125 μm. Various other circular apertures of different sizes are available as well.

The next element is an off-axis paraboloid mirror (2). This mirror is designed to reflect the light from the entrance aperture on to the Echelle grating (3). The off-axis paraboloid shape gives the mirror six degrees of

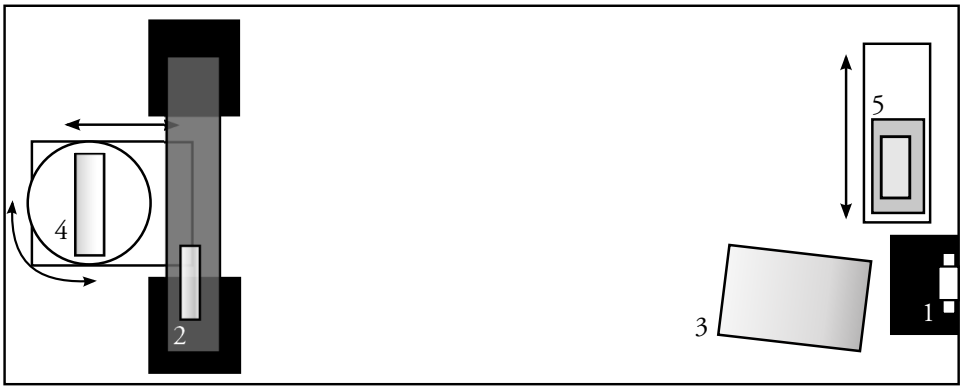

Figure 2.1: Overview of LOVES optics setup. The table below lists the numbered components in the figure.

#	Component
1	Entrance aperture mount
2	Off-axis paraboloid mirror
3	Echelle grating
4	Order-sorter grating
5	Detector CCD

freedom which makes aligning it properly difficult. A misaligned mirror will make the final image on the detector distorted.

The Echelle Grating and Order Sorter Grating

The main dispersive element of LOVES is its echelle grating. Table 2.1 lists the parameters of echelle gratings discussed in section 1 for LOVES' echelle along with ϕ, the angle of incident light relative to the normal of the grooves' short surface. Additionally, the LOVES echelle's ruling is such that the long edge of the grooves, t, is twice the length of the short edge.

Table 2.1: Parameters for our echelle grating and instrument setup.

Parameter	Value
ϕ	6.5°
θ	63.43°
d	32.25μm [1]

In addition to its echelle LOVES has a cross-disperser, called and Order Sorter Grating (OSG) as well. The OSG of LOVES (4 in fig. 2.1) is a standard concave reflection grating mounted on a rotating table, which in

[1] Given as 31.005 mm^{-1} by the manufacturer

turn is mounted on a translation table. This enables it to both adjust focus on the detector by moving towards and away from it and change the wavelength on the detector by rotating. We can rewrite the grating equation, eq. 1.1, to calculate its dispersion.

$$sin(\beta) = -sin(\alpha) + m\frac{\lambda}{d}. \tag{2.1}$$

Where α and β are the angles of incoming and outgoing light rays. m is the order number. In our case, we are always looking at the OSG's order 1. λ is the wavelength of light and d is the distance between grooves in the grating and is usually given as the grating constant $k = d^{-1}$. For LOVES's OSG we have $k = 900/\text{mm}$.

Detector

The detector of LOVES is a 4100 by 2098 pixel back-lit CCD with a pixel size of 12.5μm. It is connected to a pc via a sequencer. The sequencer and readout systems of the CCD also come with a piece of software to read out the CCD called IOUSBCCD which will be described in more detail in section 3.4.

The CCD is mounted on a translation table, much like the one the OSG is mounted on. The biggest difference between the translation tables is that the CCD one is geared to move a smaller distance with each step of the step motor than the OSG table. The step size is only 0.25μm meaning that it takes about 50 steps to move the image by one pixel. This is useful for very fine control of where spectral lines end up in the image.

The CCD needs to be cooled. At room temperature it saturates in seconds from thermal electrons alone. The cooling system is very simple: it's a copper block through which liquid nitrogen (LN) can flow. The CCD is mounted on this copper block with thermal paste so it cools down as the LN flows through the block. The LN comes from a thermos mounted on the outside of the tank and proceeds to boil off at the other end of the tank after going through a hose from the detector.

The CCD has several imperfections and defects. These defects are mainly single and columns of hot pixels, pixels that always show a higher signal than surrounding ones. From experience with the instrumentation it has been determined that some of the prominence of these features is lessened when the CCD is cooled aggressively. The CCD is at its best when at, or close to, the temperature of LN, roughly -196°C. An image with the CCD at this temperature is shown in fig. 2.2. Due to the downscaling of the resolution in order to fit in this document, single hot pixels are impossible to make out. A more detailed comparison between a fully cooled CCD and a warmer one can be found in fig. 3.5.

Figure 2.2: 10 second exposure of the CCD without a light source. The CCD was cooled to roughly -196°C when the exposure was taken.

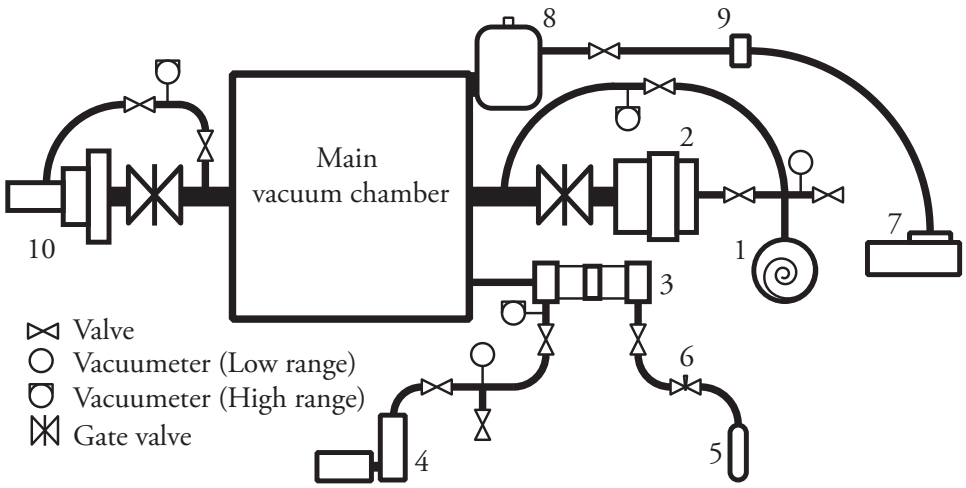

Figure 2.3: Schematic picture of LOVES vacuum system. See table 2.2 for a list of components.

Furthermore, in fig. 2.2 a slow variation in the background intensity vertically across the image is discernible. This variation is about 10 or 20% between the highest and lowest background intensities. There are indications that the sensitivity of the detector to light varies across the surface as well. However, at the point of writing it is hard to confirm this as detailed analysis have only been done on a single image and the intensity variations in the spectral lines could be caused by differing line intensities at differing wavelengths. These concerns are not critical for this project since it does not rely on line intensities for any of the results.

2.2 Vacuum System

Since LOVES operates in the ultra-violet, the optical path needs to be evacuated, as discussed in section 1. For this purpose LOVES has a vacuum pumping system that is capable of evacuating a $1m^3$ vacuum tank and keeping it at a pressure of 5×10^{-5} mbar. A schematic image of the vacuum system can be seen in figure 2.3.

For the rest of this section, a number in parentheses (n) will refer to a number in table 2.2 and figure 2.3 to ease the description of the vacuum system.

Figure 2.3 has 4 symbols other than numbers, described in the lower left. There are two types of valves and two types of vacuumeters. The normal valves come in a couple of different configurations and makes, but all do the same thing: they open or shut the flow of gas at that point. The larger gate-type valves are a bit different from the normal ones and are used as seals on the main chamber. Additionally they differ from the normal valves

Table 2.2: List of components in figure 2.3. Numbers correspond to numbers in that figure.

#	Component
1	Scroll type fore-vacuum pump
2	Turbomolecular pump
3	Hollow cathode lamp
4	All-in-one pumping station (turbomolecular + fore-vacuum pump)
5	Carrier gas supply
6	Needle valve
7	Diffusion pump
8	Liquid nitrogen container for cooling system
9	Filter
10	Cryo pump

in that they are not manually operated. They are instead pneumatically actuated.

The two different types of vacuumeters are different in the pressure range at which they operate. The low-range type operates down to a pressure of roughly 1×10^{-3} mbar while the high-range one is a combination of several types of probes and works from atmospheric pressure down to well below our operating pressure.

The primary pumping system of the tank consists of (1) and (2). (1) is the fore-vacuum pump which is used to first pump the main chamber down to a pressure of roughly 1×10^{-2} mbar. At this point (2), the turbomolecuar pump (turbo pump), can start operating. When the turbo pump is turned on, the fore-vacuum pump stops pumping directly from the main chamber and works instead at pumping away the air that the turbo pump expells. The turbo pump brings down the pressure of the chamber to about 5×10^{-5} mbar. In theory, the turbo pump should be able to get the pressure lower, but due to the large volume of the main chamber and the multitude of flanges and couplings in the system, the operating pressure is 5×10^{-5} mbar which is an acceptable operating pressure. At the far end of the tank, at (10), there a cryo pump, forming a condensation trap to avoid condensation on the cooled CCD. However, the cryo pump is currently not in use and is disconnected. A vacuumeter is mounted by the cryo tank to measure the pressure at the far end of the tank, which normally differs from the pressure at the pumping end by about an order of magnitude.

The system containing (3) through (6) is the light source, the hollow cathode (HC) lamp. Details on the HC can be found in section 2.3. The HC pumping system is designed to allow window-less access to the optics in the main tank. To allow for this it needs to be possible to let the carrier gas of the HC to be continuously supplied since a small amount is constantly

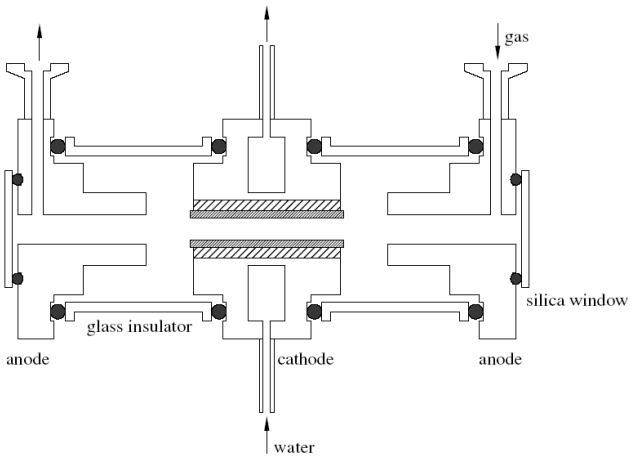

Figure 2.4: Cut-through image of the hollow cathode lamp. Image courtesy of Ulf Litzén.

flowing into the main chamber via the entrance slit. The needle valve, (6), on the carrier gas supply allows for this. The other components here are rather intuitive regarding what they do. The pumping station, (4), contains both a small turbo pump and a fore-vacuum pump and pumps out the air of the HC to make it possible to fill it with the carrier gas. (5) is a gas canister supplying whatever carrier gas might be needed.

Finally, there is a single fore-vacuum pump (7) that creates a vacuum in the thermos (8) used in the cooling system to house LN. This line also has a small filter (9) to protect the pump from dirt.

2.3 Light Source

The light source is an integral part of spectroscopy. LOVES can mount and use a variety of different light sources depending on the requirements of the current experiment. For this project, however, we have exclusively been using a hollow cathode (HC) lamp. The reason for this choice is that a HC produces very sharp spectral lines (Edlén, 1963), which is beneficial for accurate wavelength measurements. The HC lamp is a gas discharge lamp with the added benefit that metal spectra can be added to its gas discharge.

A cut-through image of the HC can be seen in figure 2.4. It consists of a chamber filled with a carrier gas, usually neon or argon. When other gas lines are desired, a small amount of another gas can be mixed into the carrier gas as well. On each end of the lamp there is an anode with a hole for either supplying or extracting gas. The middle of the lamp contains the cathode, from which the HC derives its name. This cathode is made out of the material, usually a metal, that one wants to study. The middle part of the lamp has a channel for water to flow through to cool the lamp down as

the cathode gets hot during operation.

The lamp works by applying high-voltage between the anodes and the cathode. This accelerates the small amount of free electrons that are always present in any gas towards the anodes. On the way they collide with the carrier gas atoms which are ionised by the collisions. The newly produced free electrons goes on to help form further new ions. The newly formed ions, however, are accelerated towards the cathode where they collide with it. The collisions knocks metal atoms out of the cathode, a process known as sputtering. The sputtered atoms are excited in interactions with the carrier gas and sends out light as they de-excite. This provides the light from the hollow cathode. Along with a spectrum from the cathode metal, spectra from the carrier gas and any present impurities are present in the light from the lamp. This is because not every interaction with a carrier gas atom results in an ion. Many result in excited atoms, making the carrier gas glow along with the sputtered metal atoms.

The HC is typically operated at a pressure of a few mbar, a voltage of slightly below 1000 V and a current of a few hundred mA. The operating pressure is dependent on the carrier gas, however, with neon at roughly 1.3mbar and argon at 0.4mbar. These values should be taken as guidelines, since optimising them can have a significant impact on how the HC performs.

Chapter 3

Operating LOVES

This section is written as a users manual for LOVES, intended to be used as a resource for anyone who might want to operate LOVES. As such, this chapter contains sections on how to, e.g., run the vacuum system, open the tank or use the CCD.

3.1 Opening of the Vacuum Tank

The LOVES vacuum tank is a roughly 2.5m long aluminium tube with a diameter of 0.7m that can be opened at both ends to access the internal components. The tank can clearly be seen in fig. **??**. Opening the tank should only be necessary if realignment or maintenance of some sort is needed on any of the internal components.

Precautions Before Opening

Before opening the tank it should be vented, i.e., filled it with air. Venting it should preferably be done fairly slowly as a too rapid increase in pressure can cause condensation of water vapour on optical surfaces or the sensitive detector. One should also make sure that the detector itself has heated up after being used or it will function as a cold-trap and condensation will preferably form on it rather than other warmer components. Venting of the tank should be done via the venting valve close to the fore-vacuum pump and one should ensure that the turbo pump is closed off from the air flow. While it's possible to vent through the turbo pump, it's preferable to be on the safe side and not subject it to large volumes of high-speed airflow.

Opening the Tank

The vacuum-pump equipped side of the tank is the right side of fig. 2.1 and therefore allows access to the detector, entrance aperture and echelle

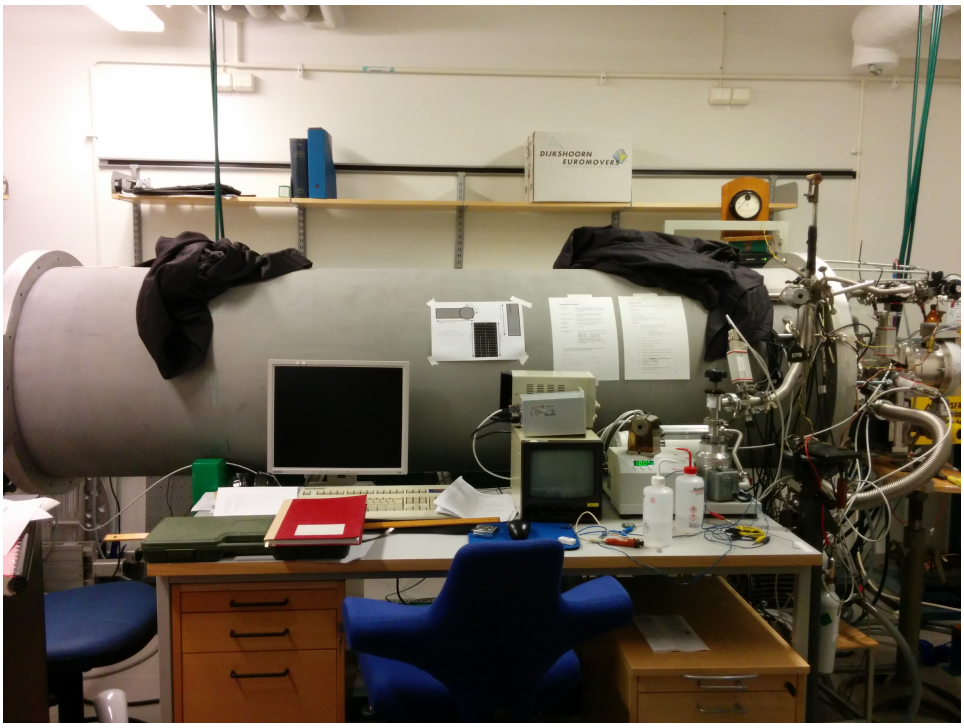

Figure 3.1: Photograph of LOVES.

grating. The opposite side allows for access to the order sorter grating and paraboloid mirror.

When opening the ends they should be supported from below. This is because the hinges can hold the doors themselves but both ends have various apparatuses mounted which means they weigh significantly more than the door alone. This is especially true for the side with the vacuum pumping equipment. This side also has throughputs for power connections to step motors and detector signal that need to be disconnected before opening. Be especially careful with the detector signal connections to not introduce high voltages via static charges. Stay grounded at all times when handling these! There is a grounded plug with all 24 pins soldered together hanging by the external connectors that should be on whenever the ordinary plug is not connected.

3.2 Operating the Vacuum System

The vacuum system is described in section 2.2. This section will make use of fig. 2.3 to refer to numbered components in that figure. This section will detail how to start up and run the pumping system.

Normal Pumping Operation

The two vacuum pumps in the system should be running at all times while LOVES is in use to preserve a low enough pressure. Since it takes upwards of 24 hours to reach operating pressure of $\sim 10^{-5}$mbar in the tank from atmospheric pressure the pumps should be left on if the instrument is to be used again in the near future. During use of the turbo pump the cooling water for it needs to be running. This is turned on in the adjacent room by the sink, using a valve labelled "echelle turbo". A slow trickle of water from the outlet hose is enough to cool the pump and ensures that as little water as possible is wasted.

Starting Up the Vacuum System

Assuming the tanks starts out with a fully vented, and at atmospheric pressure the first thing to do is to use the fore-vacuum pump (labelled 1 in fig. 2.3) to start off the pumping. Before turning the pump on, the valves in front of and behind the turbo pump should be closed since it's unnecessary to subject the turbo pump to comparatively high-pressure airflow. Once the pressure in the tank has dropped to between 10^{-2} and 10^{-3}mbar the turbo pump can be turned on. To do this, first open the valves by the turbo pump and the close the valve directly between the fore-vacuum pump and the tank and start up the turbo pump. Don't forget the cooling water! It will take a few minutes to reach normal operating frequency of 549 Hz but the pressure in the tank drops rather quickly after it has been turned on.

There is a small vacuum pumping station set up for use with the hollow-cathode lamp, as can be seen in fig. 2.3. Use of this will be covered in section 3.3 below.

Pressure Gauges

The vacuum system has three vacuumeters installed at different points to measure the pressure in the tank. The one usually used to measure the tank pressure is the one mounted on the vacuum-pumping end of the tank, closest to the turbo-pump. This one is assigned to channel two on the vacuumeter controller. In addition to this one there is a low-range one close to the fore-vacuum pump, assigned to channel one, which cannot handle pressures under $\sim 10^{-3}$mbar and is usually used to determine how well the turbo-pump is working. If the turbo pump works correctly pressure at this vacuumeter will rise when the pump is turned on. Finally, there is one vacuumeter at the other end of the tank, assigned to channel four. This vacuumeter was installed to see how much of a pressure gradient there is in the tank.

3.3 Using the Hollow-Cathode Lamp

The workings of the hollow cathode lamp are detailed in section 2.3. This section is about how to assemble and use the HC.

Assembling the Hollow Cathode Lamp

Assembling the HC can be a bit fiddly and usually requires two people. The lamp consists of five main pieces, two anode pieces, one cathode piece and two glass insulators. If the glass insulators are blackened on the inside they should be cleaned with weak hydrochloric acid before assembly. The blackening is sputtered metal that has stuck the inside of the glass insulators. In the worst case scenario the whole length of the glass tube can become coated which would short-circuit the lamp. The sputtered surface has a tendency to accumulate gas and contaminants which can make the discharge unstable. Clean glass insulators are always preferable to blackened ones if available. Between the glass insulator and the anodes and cathode there are rubber o-rings to seal the lamp from the outside atmosphere. Since the lamp operates at pressures lower than atmospheric it automatically seals when it's in use. In order for the HC to not fall apart when at atmospheric pressures there is also a pair of threaded rods that hold the lamp together using nuts screwed onto them, holding the whole thing together.

Preparing the Hollow Cathode for Use

When the HC is assembled and mounted on the tank a high-voltage power supply is needed. Furthermore, a ballast for the circuit is needed. This is to reduce and stabilise the current flow through the lamp. This is important because high or fluctuating currents make the lamp very unstable and prone to random flashes. When the HC is evacuated it needs to be filled with a carrier gas. This is done via a small pumping station next to the computer in front of the vacuum tank. This pumping station incorporates both a fore- and turbo vacuum pump so it only needs to be turned on to evacuate the lamp. When the lamp is evacuated it needs a supply of gas. This is generally done by first filling the tube from the gas canister to the HC and then closing the supply. This leaves more than enough gas to fill the HC to normal pressure and prevents the gas canister from draining too quickly. Normal pressure in the lamp depends on the carrier gas. The two most common gases are neon and argon. Pressure for neon is around 1.3mbar and for argon it is 0.4mbar. The vacuumeter on channel five is used to monitor the pressure in the HC.

Before turning on the HC it is important to turn on the cooling water for it. The cooling water can be turned on in the same place as the cooling water for the turbo pump: in the adjacent room at the sink. The tap is

labelled "echelle HC". If the cooling water is not turned on the water that fills the hose will start to boil and eventually destroy the hose, leading to leaks.

Using the Hollow Cathode Lamp

When everything is set up you can turn on the power supply and set the voltage to $\sim$ 900V and then slowly up the current until the lamp lights. The colour of the lamp depends on the carrier gas used. Neon will give a deep orange glow while argon will give a bright blue. A pinkish colour in neon or a greenish cyan for argon usually means that the HC is rich in contaminants, which usually happens in a newly assembled HC. These contaminants will be depleted over time and the colour of the glow will usually trend towards a more pure carrier gas colour as time passes. A newly assembled lamp can also be a bit unstable and prone to flashes initially. This is usually due to tiny flecks of material that gets stuck on the various parts and can often be seen as a bright spot somewhere on the anodes or the cathode. Running the lamp for a while usually gets rid of these as they get sputtered away by the discharge.

When using the HC with LOVES one can use it in two different ways. LOVES entrance aperture has a slider mounted on it that can be set to three different positions. These are, from top to bottom: window, closed and open and are marked by the little rod that one uses to change the position. The closed and window settings are identical when it comes to HC operation. Neither allows gas to flow into the tank, so one can set a pressure level of the cathode and run it for several hours without worrying about the pressure in a well-sealed HC. The alternative is to run the HC with the aperture open. This means that the carrier gas will continually leak into the tank through the entrance aperture. The volume of gas that's leaking into the tank is negligible in the large volume of the big tank and is pumped out very quickly. It is, however, a significant loss of gas for the lamp. This means that gas will continually be flowing through the HC. In the optimal case it will flow out equally fast as it flows in. The outflow cannot be adjusted, so the solution is to moderate the inflow. This is done via a needle valve on the HC that can fine tune the inflow of gas in order to keep the pressure in the HC constant. This can get very fiddly and getting a stable pressure is quite hard, but definitely possible. The advantage of an open aperture is that one can see fainter lines in the spectrum, especially far into the UV-region since the window starts to absorb a fair amount of light in the UV.

3.4 Detector and the Optics System

This section is about how to operate the translation and rotation tables that seat the order sorter grating (OSG) and the detector. The section also details how to read out the CCD and what software settings are useful for this.

Step Motors and Translation Tables

LOVES contains three step-motor driven tables that control the rotation of the OSG as well as its distance from the detector and the detector's position perpendicular to the OSG. See fig 2.1 for an overview. Each one of these step motors can be driven individually. The motors are driven with 5V and the current flowing through them can be measured by an Ampere-meter. The motors use the most current when standing still so looking at when the current goes up is a good way to tell when they are done moving. Each step motor is controlled via a microchip that is soldered to a control board made by Sven Huldt. These controllers are then connected to COM-ports three through five on the instrument computer. There is an information taped to the tank that details the numbering of the motors and what ports they are connected to along with a schematic of components in the tank.

Commands can be sent from the computer in two ways: either via a set of small wrapper programs run from a command line or directly via a COM-port terminal. For both of these options the information sheet taped to the tank detail what commands are available and what they do. The set of programs is usually the recommended way to use the motors, as it is impossible to do things like reset internal step counters with them. This is good since recalibrating the step counters is quite a bit of work.

The motor controlling the translation of the detector is geared so that one step is smaller than one step for the motors on the OSG table. This is because one pixel on the CCD is $12.5\mu m$ and you need to be able to step the detector on those scales. Motor 1, the detector motor has a step size of $0.25\mu m$ so 50 steps is one pixel. Being able to move on such small scales is useful for e.g., avoiding bad pixels. The two OSG motors , motors 2 and 3, are more used to get properly focussed lines on the CCD so they should generally not need to be used. They have a step size of $3/400°$ and $2.5\mu m$, respectively. All these numbers are detailed on the information sheet much like the list of step motor commands.

Cooling the CCD

Before being useful, the CCD needs to be cooled down. A room temperature CCD will be completely saturated by thermal electrons even at the shortest exposures. The cooling system is quite simple: it is essentially a copper

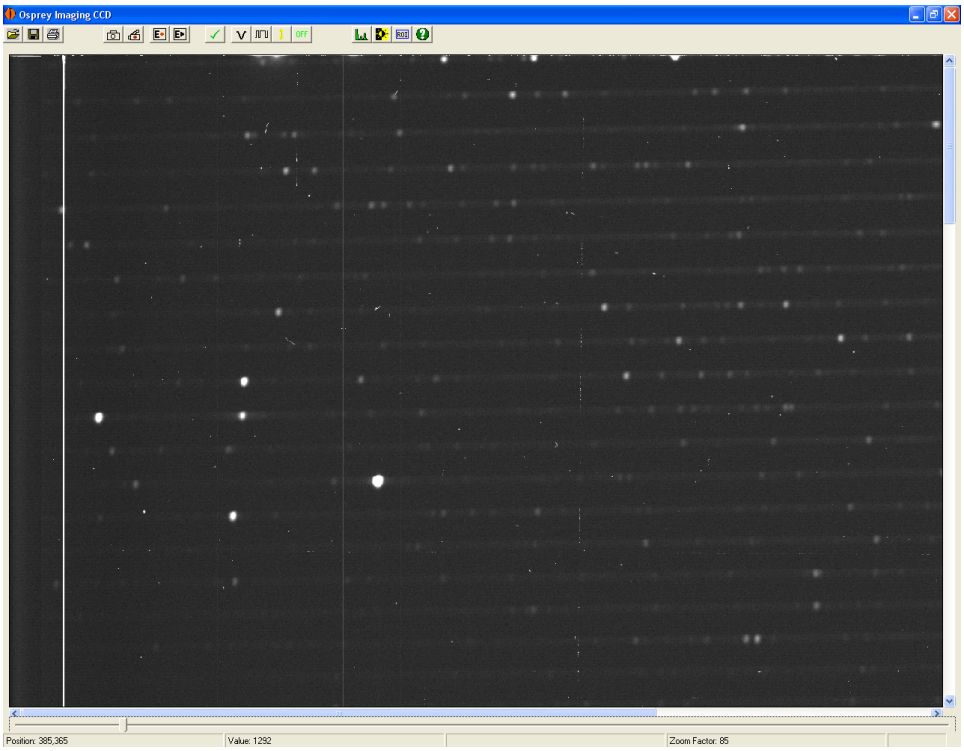

Figure 3.2: Screenshot of the OIUSBCCD interface.

block that the CCD is fastened to. The block has piping running through it and through these pipes liquid N_2 is poured. On the outside of the tank, by the vacuum pumps, there is a thermos that one fills with liquid N_2 which then boils through a hose connected to the CCD cooler block. Excess N_2 subsequently boils out of an outlet on the far side of the tank. There is currently no way to monitor the temperature of the CCD. The best way to get an idea about how cool the CCD is is to read it out and look at the image.

Using OIUSBCCD to Read Out the CCD

The CCD readout is done using the instrument computer. The CCD is connected to the computer via a sequencer. The sequencer, in turn, is connected to the CCD via two BNC cables, one for each readout channel.

The sequencer and software (OIUSBCCD) for the CCD were all made by Osprey Imaging. This company normally makes equipment for medical purposes so many functions of the software used to read out the CCD are not useful when using LOVES. Figure 3.2 shows the interface of OIUSBCCD.

The main view in the middle is a loaded image. This image can be either loaded from file or displayed after being read from the CCD. This area of the

interface will be blank upon first starting the program. Both vertical and horizontal scrollbars are available at the edges of the image when applicable. Below the horizontal scroll bar is a slider to control zoom level: Left is less zoom. Below the zoom are three fields that show, from left to right, the x and y coordinates of the cursor, the pixel value at the cursor and finally the zoom factor. Maximum pixel value varies depending on bit depth per pixel: 12 bits/pixel has $2^{12} - 1 = 4095$ and 16 bits/pixel has $2^{16} - 1 = 65535$ as their maximum pixel values.

In the top of the interface we have a row of buttons. These open various sub-windows where settings can be made. Note that the program lacks a standard 'ok' or 'apply' button in these windows, anything that is set is immediately applied and the window can be closed or left open without losing any settings. The first two buttons are normal load and save buttons, and they work as one would expect. Images can only be saved in, or loaded from, the non-standard *.IMG*-format that the software uses. The third button, with an icon resembling a camera, is used to expose the CCD and read out the image and will be described in detail below.

The three following buttons are for recording a set of images. This is not possible with our large CCD with its long readout times so they should not be used. The green check-mark button, number 8, is a quick initialise button that sets up default values for voltages and gain. Normally non-default values are used and this button will overwrite those values so it should generally be left alone. Next, button number 9, is a black 'v' that opens a window for setting voltages for the sequencer and CCD. Voltages can be set manually or loaded from file. Good voltages for our CCD are set up in the file '*HCCD4280.vtg*' and can be loaded using the 'load' button. Number 10 is the sequencer button, depicting a square wave. Here one sets the binning and exposure time, among other things. The sequencer window is pictured in fig. 3.3. To the top left under the heading 'CCD type' is the binning controls. The four top choices are useful binnings and can all be used depending on needs. The fields to the right update automatically to reflect binning choice. The fields under 'clocking' is the readout direction of the readout registers. These should stay on 'forward' for both horizontal and vertical registers since otherwise nonsensical images, usually almost completely black or white, are produced. The reason for this is not known, possibly some of the readout registers are damaged or broken in some way.

The next button in the interface is the gain button, button number 11. The window it opens is shown in fig 3.4, along with the controls for displaying various pixel values. The gain window is mostly used for setting the per-pixel bit depth. Higher bit depth means longer readout time and larger file size but also a more detailed reproduction of the light levels. Since the light levels are generally fairly low in LOVES 16 bits pre pixel is recommended for images that are to be used for science. Gain can also be set, but it has an extremely minor or non-existent impact on resulting images. The window

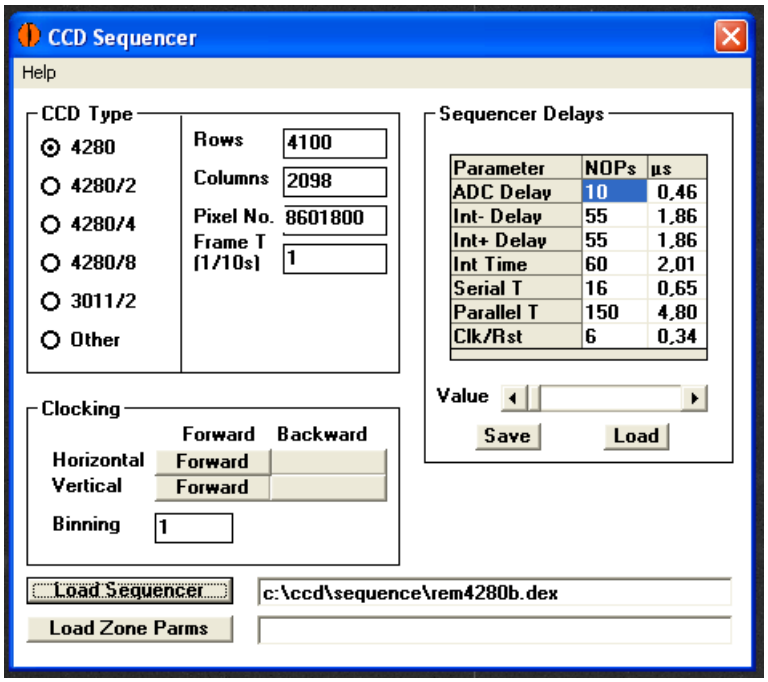

Figure 3.3: Screenshot of the sequencer window of the OIUSBCCD software.

titled 'Display LUT' is opened via the button in the interface with a light bulb on it, button number 14. These two sliders represent the maximum and minimum pixel values to plot. The useful range of values in our images are typically very small and at a very low level (between 1000 and 4000 using 16 bits/pixel or 200 and 600 for 12 bits/pixel). This means that normally the sliders should be like in fig. 3.4: very close together and close to the top. While a numeric input would be very useful, one is not supported by the program so one has to wrestle with the sliders a bit.

The last useful button in the interface is the ON/OFF button, button number 12. This button will, unintuitively, be green and say 'OFF' when the CCD is turned off and switch to being red and reading 'ON' when the CCD is on. Note that the software has no way of knowing that the CCD is actually on or not, it merely switches between the two states when clicked, Giving an error message when it cannot communicate with the CCD. The sequencer emits an audible click when switched on or off, however, so it's possible to tell that it actually switched state.

The remaining buttons: the green histogram and the 'ROI' buttons are both features that are never used by us. The last button is a simple about button that states what version the software is, when it was made and by whom.

If reading out a large image or making a long exposure, the program will appear to be unresponsive throughout the exposure and readout. Crashes

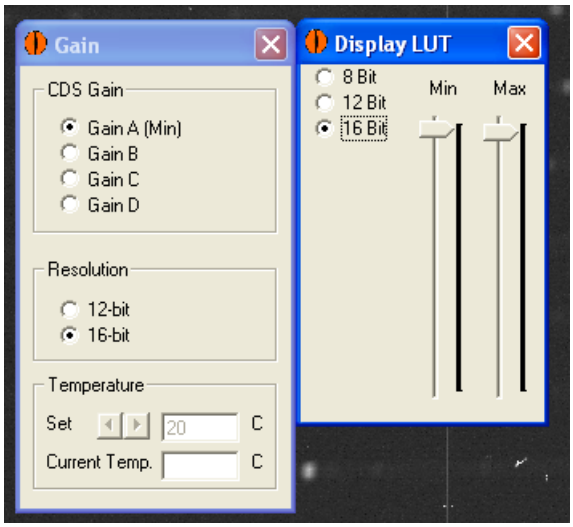

Figure 3.4: Screenshot of the gain and pixel contrast windows of the OIUS-BCCD software.

can and do happen during this time and they are indistinguishable from normal operation so it's useful to keep track of the time required for an exposure. On top of the user-defined exposure time, the readout time of the CCD depends on the binning factor. An 8-binned exposure reads out in a few seconds at most while a non-binned exposure takes several minutes.

As mentioned above, the best way to determine if the CCD is cool enough to use is to expose it and look at the image. This is best done with a binning of 8 since that avoids long readout times. Figure 3.5 shows two images, first subfigure 3.5*a* that shows a relatively warm CCD and then subfigure 3.5*b* that shows a fully cooled CCD with as good an image as is possible to get.

Note that the vaguely horizontal hot pixel patterns visible in fig. 3.5*a* as well as the hot columns are reproducible and can thus be mitigated by subtracting a dark image during image processing. Having a cooler CCD is always preferable since less data is lost.

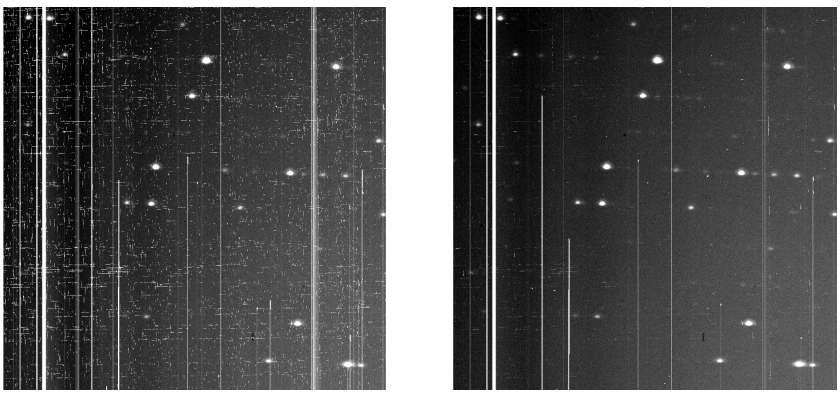

(a) Not fully cooled CCD (b) Fully Cooled CCD

Figure 3.5: Two partial images read out from the CCD at different temperatures. Note how columns of hot pixels are disappearing going from warmer to cooler. General background level is also reduced.

Chapter 4

LOVES Hardware and Software Development

At the start of the project LOVES had been unused for several years.In addition, the lab changed locale just around the start of the project. This means that LOVES was almost completely disassembled and the act of moving it one floor down into the basement of the observatory meant the optics had to be realigned and refocussed. Because of LOVES being disassembled we took the opportunity to build an entirely new vacuum system, as described in section 2.2. This means that a rather large amount of time was spent on making sure that the hardware was functioning as intended in its new location. The vacuum system detailed in section 2.2 was assembled from the ground up. Parts of it was added as needed during the course of the project.

Several software scripts and programs have been developed during this project to enable LOVES data reduction. All but one of these were realized using the Python scripting language, relying on the Numerical Python module, or NumPy. Of note is the Scientific Python module, or SciPy, which has provided e.g., the least square fitting algorithm used in the order fitting process. The last program, the image file converter, was written in C. The image file converter was the first piece of software that was written, before a switch to python due to being easier to use was made. In addition, this section includes descriptions of some scripts that were made and found to be non-useful and thus abandoned, such as the Fourier Transform filtering script. Detailed description of what all scripts do are provided in the sections below.

In addition to these bigger pieces of code, several smaller scripts were written for single instances of fitting or plotting. Since these are neither very large or especially complex, they will not be detailed here.

4.1 Optics Alignment and Focussing

In order to move the large vacuum tank safely all optics were taken out and moved separately. While guides were left on the optical table these are never perfect so the light path had to be aligned. The alignment was done by installing the optical components one by one along the light path (described in section 2.1, especially fig. 2.1). A fairly large circular entrance aperture along with a bright standard light bulb was used as a test light source. Alignment is then a matter of making sure that the light falls onto the next component in line until a visible reflex is noticeable on the detector. This procedure gave us an image on the CCD, however the spectral lines (or images of the slit) were badly unfocussed.

In the ideal case, the spectral line on the CCD should be a perfect image of the entrance aperture. With the standard aperture this is a circle. The initial focussing was done by using a very bright lamp and using the reflectiveness of the CCD to project the reflex from it through a pair of binoculars. The element that is the hardest and most crucial to focus is the paraboloid mirror. It is hard to focus since it is asymmetric, with six degrees of freedom, and needs to be mechanically moved by micrometer screws on the back. It needs to not be moved from its position during this procedure. Since the mirror is standing on a bar above the OSG about half a metre into the tank this can get difficult, especially when a lot of turning of the screws are required. Once the image is focussed the projection from the binoculars looks like a small, sharp circle rather than an ellipse with one or more sides blurry.

The final focussing step is to take images of spectral lines using the CCD and moving the OSG until they are as round and sharp as possible. Fortunately, only OSG translation affects the focus so the procedure is fairly simple. It is quite time consuming due to long CCD readout times, however, since unbinned images are needed.

Fig. 4.1 shows a few examples of the images that were used for focussing. Note how the individual lines stretch in the horizontal direction with higher step count and in the vertical direction with lower count. Best focus was found to be at 11550 steps, which was then redefined as the 0 steps point for the OSG.

4.2 Detector

The detector existed more or less as it is today at the start of the project. However, during a period early on we suspected it had been damaged while moving the instrument. The initial testing images were full of bad pixels and were not of the same quality as pre-move images. So to test it we built a small test vacuum chamber. Testing showed nothing wrong, however, so

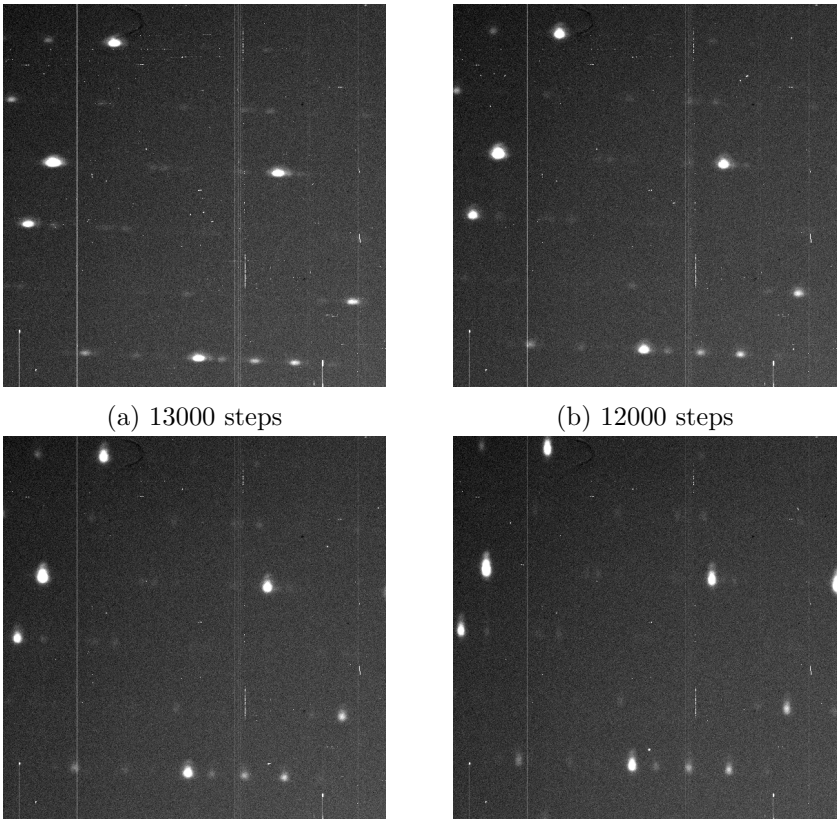

(a) 13000 steps (b) 12000 steps

(c) 11000 steps (d) 10000 steps

Figure 4.1: Four partial images showing the effect of moving the OSG for focussing. Captions for individual images indicate what the OSG step motor counter was on. One step is 2.5μm, which makes total movement from 4.1a to 4.1d 7.5mm.

after a while of testing various lamps and cooling the CCD to various degrees it seemed as though it worked fine. The problem could likely have been that the hose connecting the LN thermos to the CCD was quite a bit shorter than in the large LOVES tank. This means that it takes quite a bit more LN and time to cool the CCD in the main tank, which initially threw us off. The CCD image quality degrades very quickly with increasing temperature, so an insufficiently cooled CCD in the main tank would at first seem broken.

4.3 IMGtoTXTscript.py - Image File Conversion

This script is used to convert the *.IMG*-files that the CCD software (OIUSD-CCD) saves in into a text file matrix for further manipulation. The python script is a wrapper around a C program that does the conversion. The reason for this wrapper is that the C program only converts one file per execution so a python wrapper is used to enable the conversion of several files at once. The python script uses a separate text file called '*input.txt*' located in the same folder as the script for a list of input files. The input file should contain one file to be converted on each line, its location specified either as relative to the script's directory or absolutely. It is possible to have comments in the input file. Comments should be preceded by a hash sign (#).

The C program is called *IMGtoASCII.exe* and was purpose built to convert thee files into text matrices. On closer inspection, the *.IMG*-files turned out to be binary lists of pixel values in a little-endian[1] configuration. This was initially confusing since reading the numbers the wrong way produces strange pixel values. Additionally, the *.IMG*-files contain a 12-byte header containing the number of bits per pixel and a string identifying the origin of the code library that created the file. The program supports both 12 and 16-bits per pixel *.IMG*-files and will automatically identify them based on their header. Additionally, there is full error handling and the program will display useful error messages at most points of failure.

4.4 MakeImage.py - Useful Image Production

This script is designed to produce image files in standard image formats that are viewable using common software. By default, the program uses *input.txt*, the same file as *IMGtoTXTscript.py* uses to find input files. The correct procedure is to first run *IMGtoTXTscript.py* and then run *MakeImage.py* as the latter will fail if it fails to find the .dat files created by *IMG-*

[1]Endianness is a concept in computer science relating to how numbers are stored and read in memory. Little-endian means that the least significant digit of a number is stored and read first. Contrast normal decimal numbers where the least significant digit is stored/read last (big-endian)

toTXTscript.py. There are two required parameters that needs to be specified when the script is run: maximum and minimum pixel value to plot. The reason for this is that most common lossless image formats have problems with 16-bit pixel values. Moreover since the signal in most pixels is very low compared to the maximum possible pixel value such images would appear almost completely black. Additionally, one can override the default behaviour of using *input.txt* by using the optional parameter *-infile [filename]*. Using this parameter means only one file can be processed at a time. Finally, parameters *-h* or *--help* can be used to list all available parameters and their syntaxes. The script will output .tiff-files. If another format is needed, the file ending can be easily changed in the code.

4.5 orderfit.py - Order Fitting and Spectrum Extraction

This interactive script is used for finding the orders in CCD images and plotting their spectra. It is the largest and most complicated script that was created for this project. The point of the script is to find the spectral orders, plot their spectra and finally export the data for use in e.g., *PSFfit.py*.

Unlike the other scripts, *orderfit.py* does not use command line arguments to alter input files or set fitting options. In this case direct manipulation of the script is required. The reason for this is that this particular script has so many different input options that command line arguments would be very cumbersome. For this script, directly editing the code is simpler. The main things to change is varying the input file and its accompanying dark file. Shifting the dark file with respect to the input file might be needed if they are not properly aligned. Specifying the y-coordinates of the first two orders to be fitted is required as well. This is done with two variables, edges1 and edges2 that specify the y-coordinates of the top and bottom of a box that encloses the orders. Finally, the initial guess for the order fitting assumes negatively sloped orders. Some images have positively sloped orders which means that one has to change the slope of the initial guess. To do this there is a commented out line of code in the LineFit class that needs to replace the line below it.

Fitting Process

After reading input image and subtracting a supplied dark image the program fits the two user-identified orders. Fitting is done by first cutting the input image in the y-coordinate so that only the region around the order is available to fit in. The script then uses Scipy's *leastsq* function which is a wrapper function around the FORTRAN implementation of the Levenberg-Marquardt algorithm called *lmdif* in the MINPACK software package. The

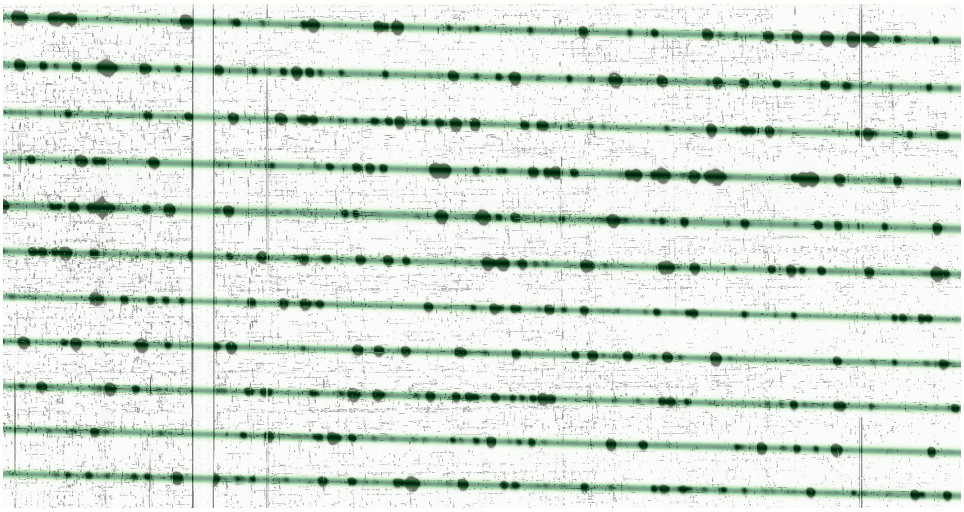

Figure 4.2: Subsection of full image showing fitted orders using *orderfit.py*. Underlying image is black-hot and fitted orders are green.

model fitted to the data can be described by two functions, a straight line, y_x, and a one dimensional Gaussian, $G(y)$, (eqs. 4.1 and 4.2).

$$y_x = kx + m \tag{4.1}$$

$$G(y) = ae^{-\frac{(y_x - y)^2}{2\sigma^2}} + b \tag{4.2}$$

The program fits the parameters k, m, a, b and σ. These are, in our CCD image context, order slope, the order's intersection with the bottom of the cut-out fitting area, Gaussian amplitude, CCD image background noise level and spread of the order width, respectively. x and y are the x- and y-coordinates on the CCD image, or in practice, of the cut out fitting area. The resulting model is a ridge of identical 1D Gaussians at every x-coordinate. An image of orders fitted this way can be seen in fig. 4.2.

After fitting the first two lines using user-supplied edges, the script asks the user how many more lines to fit. If asked to fit more lines the location of the next order is guessed using the distance between the last two. The distance between orders slowly shrink as wavelength decreases (see eq. 1.1, higher orders contain shorter wavelengths), but it shrinks slowly enough that using the distance between the last two orders is still a very good guess. Once done fitting orders the user is again asked if more should be fitted. Giving zero orders to fit starts the plotting process.

The output and plotting process first plots spectra of all fitted orders. The x-coordinate of these spectra are the distance along the order in pixel units. The y-coordinate contains an summed and normalised pixel count

number. This number is obtained for each x-coordinate by summing the values of the pixels in the y-direction as described in eq. 4.3. Where *G, a and b* are the same as in eq. 4.2. k is the maximum y-coordinate of our cut-out fitting area, which will vary from order to order. P_i is the pixel value of pixel i along the y-axis for a given x-coordinate.

$$s = \sum_{i=0}^{i=k} P_i * \frac{G(y_i) - b}{a} \tag{4.3}$$

This means that the final count in the spectra is comparable to the counts in a single pixel, but takes the entire order into account, reducing the contribution of pixel spikes. Additionally, if the script fits an unusually wide order, it will print a warning on the plotted spectrum.

Output

The script outputs several files for further use. First it plots the spectrum of each order, as detailed above, being numbered from one being the first user-supplied order to whatever order ended up being the last one fitted. Second, it plots an overview image of the whole input image with identified orders overlaid in green. This image is black-hot as opposed to the white-hot images from *MakeImage.py* to facilitate the order overlay. Third, it outputs numerical data for the orders in two files. One with spectrum counts for every order and one for order locations in the full input image. Both these are needed for specific order fitting using *PSFfit.py*.

4.6 PSFfit.py - Multiple Line Point-Spread Function Fitting

PSFfit.py is a utility for easily fitting Gaussians to identified spectral lines. It uses spectrum data files produced by *orderfit.py* as well as images from *IMGtoTXTscript.py*. The script itself uses the same fitting routine as *orderfit.py* to fit two dimensional Gaussian functions to spectral lines. The x-coordinates of these lines are provided using a plain text input file (PSFfitInput.txt by default, cf. Input.txt for *MakeImage.py* and *IMGtoTXTscript.py*) that should contain a list of approximate x-values for spectral lines in each row, separated by commas. The y-coordinates of lines are supplied from *orderfit.py* output files (see section 4.5 above). The first element of each row should be the order number that these lines are to be found in. Each row needs to have the same number of elements, so empty spaces are supported and expected since rarely do different orders have the same amount of interesting lines.

When run with appropriate inputs the script goes on to cut out small pieces of the input image around supplied coordinates. The size of this area

can be user-specified using the -sqsize parameter when running the script. It defaults to a square with 41 pixels long sides centred on the line. It then fits a 2D Gaussian function to the small cut-out area. This fitting is done with the same algorithm that is being used in *orderfit.py* and is detailed in the section about that script above. This fitting then gives accurate centre coordinates and amplitudes for each line being fitted. It also gives estimated statistical errors for each of these quantities. These errors are calculated using *leastsq* built-in covariance matrix estimation.

The script will output two images per fitted line, one with a 3D plot of the cut out square and one with the same region overlaid with the fitted Gaussian. These files are named using the supplied x-coordinate, order, image file name and lastly with a suffix of either "region" or "fit", depending on if they have the fit overlaid or not. The image will also include the centre coordinates of the fitted Gaussian along with the estimated errors. Finally, the script will save a plain text file with all the parameters of the individual fit for use in, e.g., spreadsheet programs.

4.7 useful_functions.py - General Functions

This file contains a collection of useful general functions that get called in other scripts. The reason for this file is simply to enable simple access to functions that might be useful in several different circumstances. Notable are the models used for order fitting in *orderfit.py* and the Gaussian functions for *PSFfit.py*.

4.8 Abandoned Software

At one point during the project it was discovered that there is a roughly 20% variation in the background intensity over the length of the CCD. *FFT.py* was written with the hopes of using a Fourier transform in order to filter out low frequencies from the images. In the end, the script does filtering successfully, with three different filters implemented. However, it turned out to be much too time-consuming to get the filtering to work as intended when better results could be achieved using flat-fields and dark images if needed.

Chapter 5

Wavelength Determination

The way the wavelength determination was done is by first measuring line positions using the various scripts and programs written during the project and then matching them to known line wavelengths. This procedure will be described in detail in section 5.3. Doing this enables the fitting of a function that can calculate a wavelength for any given position in an order with enough identified lines. This turns out to work well for most of the orders in the project exposure. However, some orders have too few identified lines to meaningfully fit a relevant function. Moreover, when going further into the UV it becomes harder and harder to find reliable in-order references. To show that it is possible to solve this problem a scheme where any given order's wavelength-position function can be determined using those of other orders were devised. More on this in section 5.4.

5.1 Data

The data used in this work all come from one exposure made by Hampus Nilsson on the 20^{th} of May 2003, several years before the start of this project. It was unceremoniously named "fe05201", which is the way this work will refer to it. The light source used was a hollow cathode with an iron cathode and neon at a pressure of roughly 1 mbar as carrier gas. It was running at a current of 600 mA and the CCD was exposed for 600 seconds with an open aperture to take the image. It can be seen in full in fig. 5.2. This image was chosen from a handful of other images because it contained a large amount of spectral lines and was the clearest-looking one. Additionally, The image had a dark exposure image to go along with it which helps in the data reduction.

Other exposures were made as part of the project as well. These were not analysed like fe05201 was due to having fewer available spectral line and lacking good dark images. Many exposures were taken as part of the calibration and optics focussing project as well.

5.2 Reference Lines

The source of reference lines used in this work lines is a personal collection of identified lines by Sveneric Johansson. Parts of this collection have been published in Johansson (1978) and Nave & Johansson (2013). However, Some parts have not been published due to Sveneric Johansson's passing in 2008 as mentioned in Nave & Johansson (2013). The compendium contains several thousand measured spectral lines mostly of Fe I and II, but with a tiny minority of noble gas lines and other metal lines. It covers the wavelength range from roughly 830 to 3000Å. Most of the lines in Sveneric's compendium are measured using a Fourier transform spectrometer with noble gas lines as primary references. Since this work uses the iron lines from the compendium as references they are used as secondary references. Not using primary references is unfortunate, but due to the general lack of noble gas lines in the wavelength range it is unavoidable, especially for a first time data reduction.

The identification of reference lines with measured line positions was done in two steps. The first lines that were used to fit individual order polynomials had been identified by Hampus Nilsson when the fe05201 exposure was first made. These lines are marked in app. A with an 'H'. Later on, when individual order polynomials had been fitted, another round of identifying lines was done. These lines are marked with 'P' in app. A.

5.3 Data Reduction

A flowchart of the data reduction and wavelength function fitting process can be found in fig. 5.1. The data reduction started with *fe05201.img*, a raw output image from the LOVES CCD. This image was then run through *IMGtoTXTscript.py* (see section 4.3 for details on the script) to produce a useful plaintext matrix. *MakeImage.py* was then very helpful in creating common-format images for visual inspection and deciding what to do next. For fe05201, useful upper and lower boundaries are 600 and 225, respectively. It should be noted that while this range is only about 10% of the full available intensity range of the CCD, many of the lines in the image are actually stronger than 600 in their peaks. This range is only chosen to be able to see as many lines as possible, which means adjusting it to be lower to be able to see very faint lines. The image produced by these settings can be seen in fig. 5.2.

After producing the image *orderfit.py* was used to find the different echelle orders in the image and make spectra for each one of them. Section 4.4 has information on how this order finding works in practice. The next step was to run *PSFfit.py* using the output y-coordinate data for each order from *orderfit.py* and manually found x-coordinate values for 597 spectral

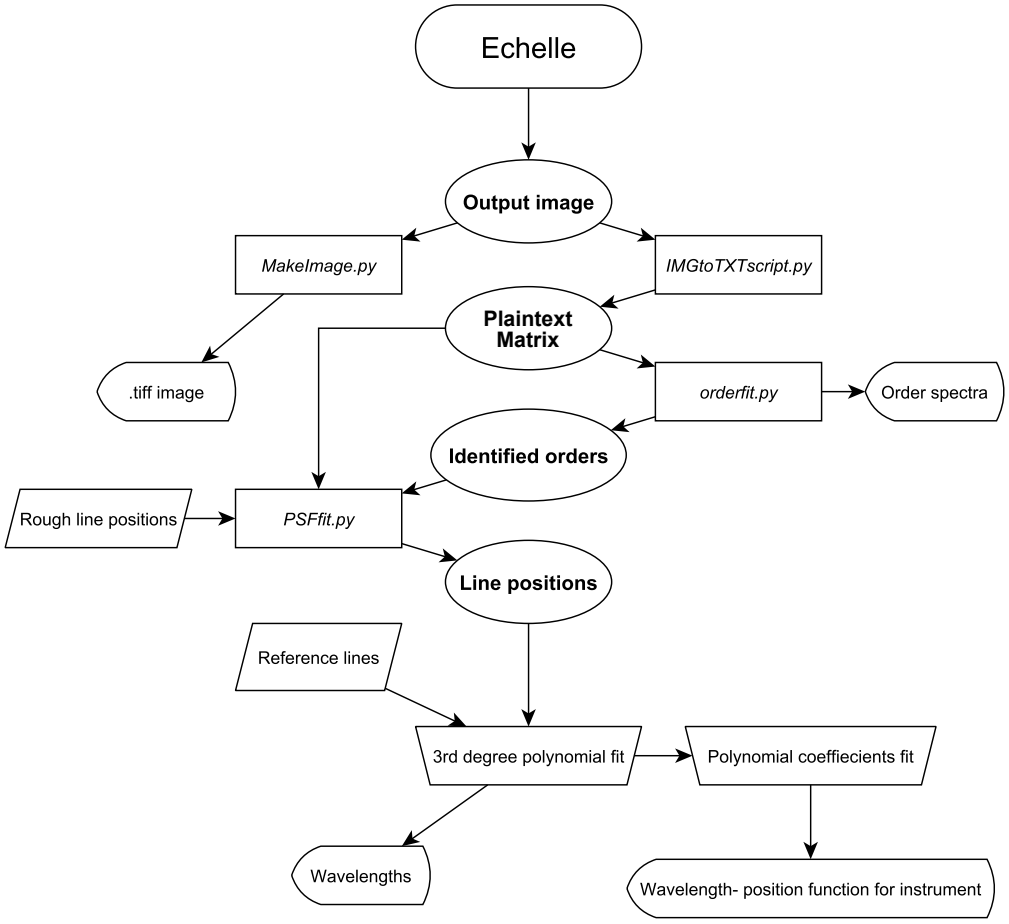

Figure 5.1: Data reduction flowchart. Ellipses represent data files, squares are scripts. Left pointing labels are outputs and trapezoids represent required external input data. The final remaining label represents a numerical fitting process.

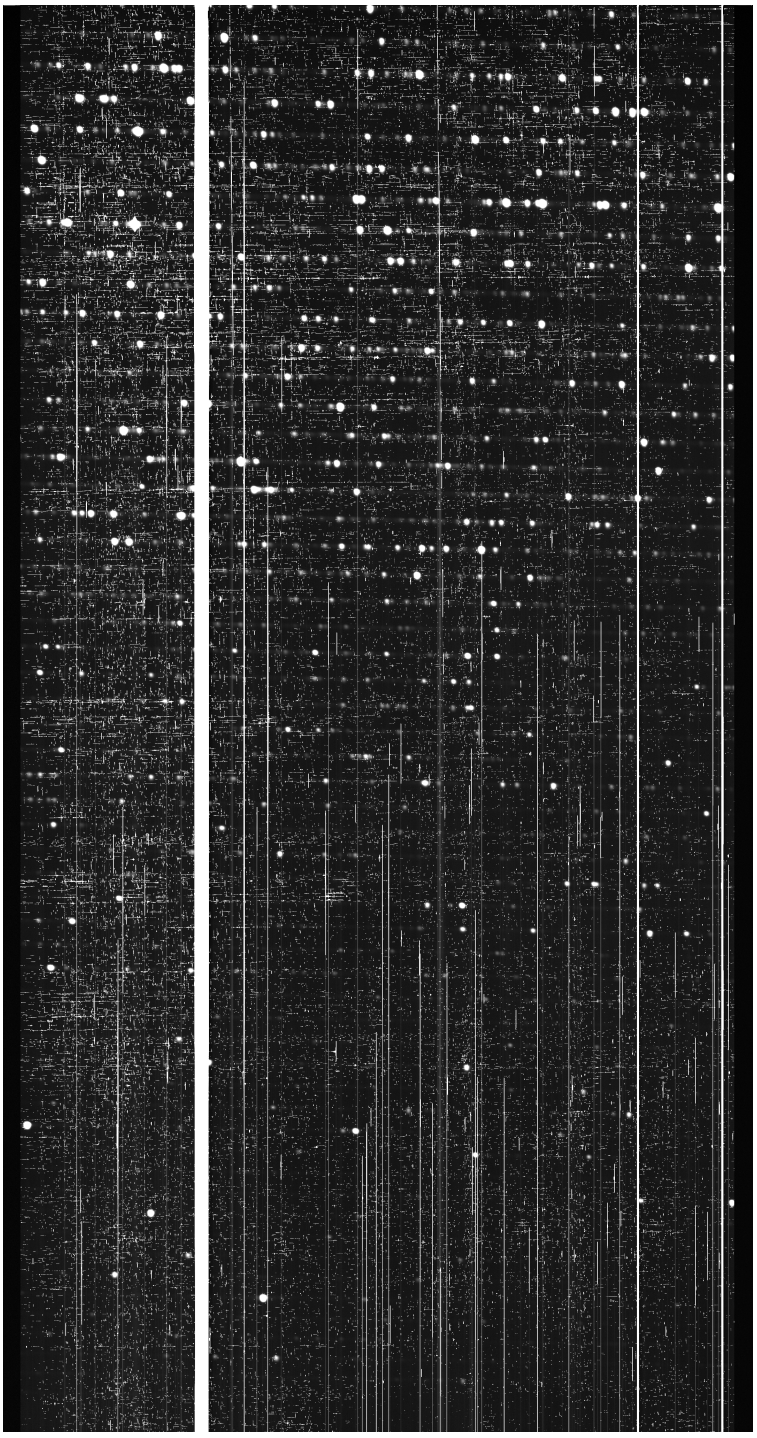

Figure 5.2: Full image of fe05201, only contrast has been set compared to raw image data. No image processing has been performed except scaling to fit on the page.

lines. These lines were found by identifying approximate line x-coordinates by eye in the image produced by *MakeImage.py*. This way of finding lines is hardly ideal, but at the time a peak-finding algorithm that could do an equally good job was not readily available and writing a new one would take longer than going through the image manually.

After running *PSFfit.py* to find accurate centroids for each line some time was taken to look into the individual fits. In this process we removed all lines whose fits are obviously faulty, e.g, the script fitted single pixel spikes or two lines instead of one. See fig. 5.3 for examples of images of the fits that where used to evaluate whether to keep the fit or not. After this process, we ended up with 461 spectral lines that have acceptable centroid coordinate values. These coordinate values were then used to compute a value denoting the distance along a given spectral order that a given line is at. This is needed because the spectral orders are inclined relative to the pixel grid on the CCD, as can be seen in fig. 5.2. The computation itself is simple. Since the orders are modelled as straight lines the distance along the order is simply $\sqrt{x^2 + (y_0 - y)^2}$, where y_0 is the y-coordinate of $x = 0$ in an order.

5.4 Fitting of the Wavelength-Position Function

Once reference lines were established it was possible to begin fitting wavelength functions to individual orders. This means that positions on the CCD could be linked to wavelengths. To begin with third degree polynomials were fitted to the separate orders. The choice of third degree polynomials is due to the fact that the underlying function is some sort of cosine function, which only has uneven terms in its Taylor series. Thus, a third degree polynomial approximates a cosine function to second order and a fifth degree polynomial would approximate it to third order. Fifth degree polynomials are not possible to use in many orders because of too few identified lines, however. Therefore third degree polynomials were used, in order to be able to fit as many orders as possible.

In general, the best fitting third degree polynomials are nearly completely linear (see fig. 5.5) and fit very well to the data points. There are a few orders where the fits are worse, notably order one and order 15 (see fig. 5.4 for order numbers). Furthermore there are six orders (5, 6, 9, 26, 31 and 32) that initially had fewer than five identified lines which makes fitting a third degree polynomial meaningless.

These individual order fits give good wavelengths for unidentified lines in the orders where they are available (see the black points in fig. 5.6). However, it would be useful to interpolate between individual orders. This would make it possible to obtain wavelengths for orders that do not contain enough identified lines or that can not have an individual polynomial fitted

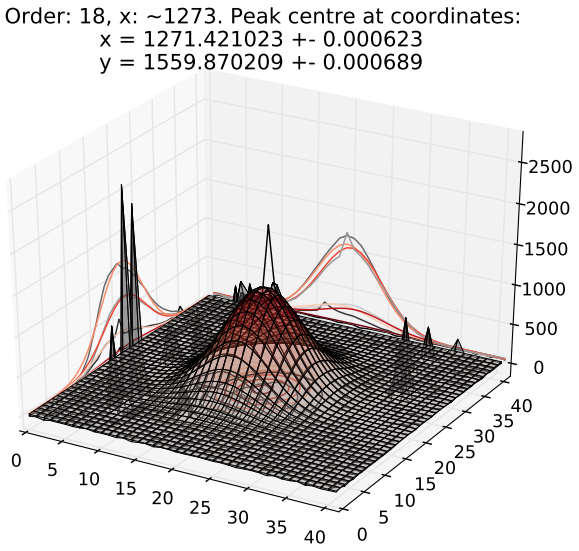

(a) Successful fit.

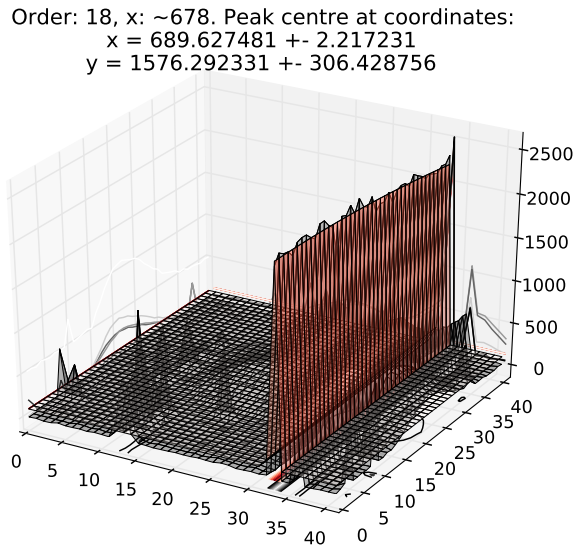

(b) Failed fit

Figure 5.3: Two examples of fits generated by *PSFfit.py*. Figure (a) shows a well-behaved fit while figure (b) shows an example of a bad fit that is unsusable due to fitting a column of bad pixels rather than the line. Error estimations on the x- and y-coordinates are based on the covariance matrix from the χ^2 fitting.

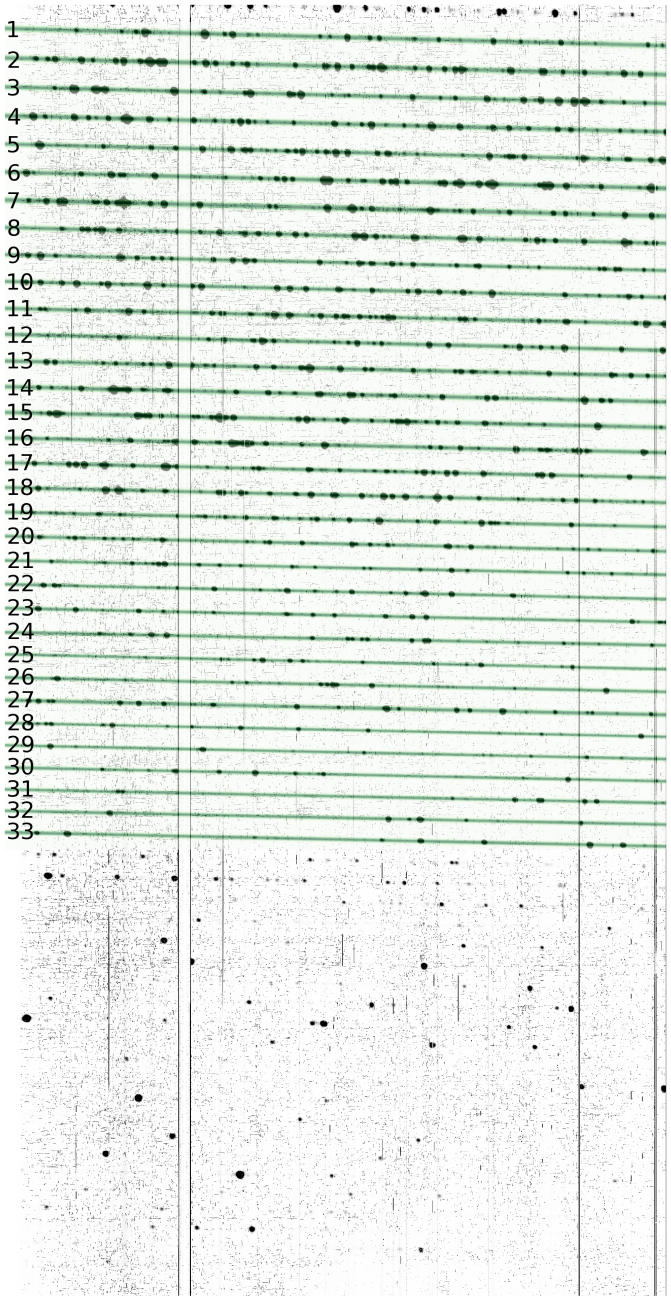

Figure 5.4: Full image of fe05201, showing fitted orders and the numbers assigned to them. A dark image has been subtracted here compared to 5.2, showing much fewer hot pixels.

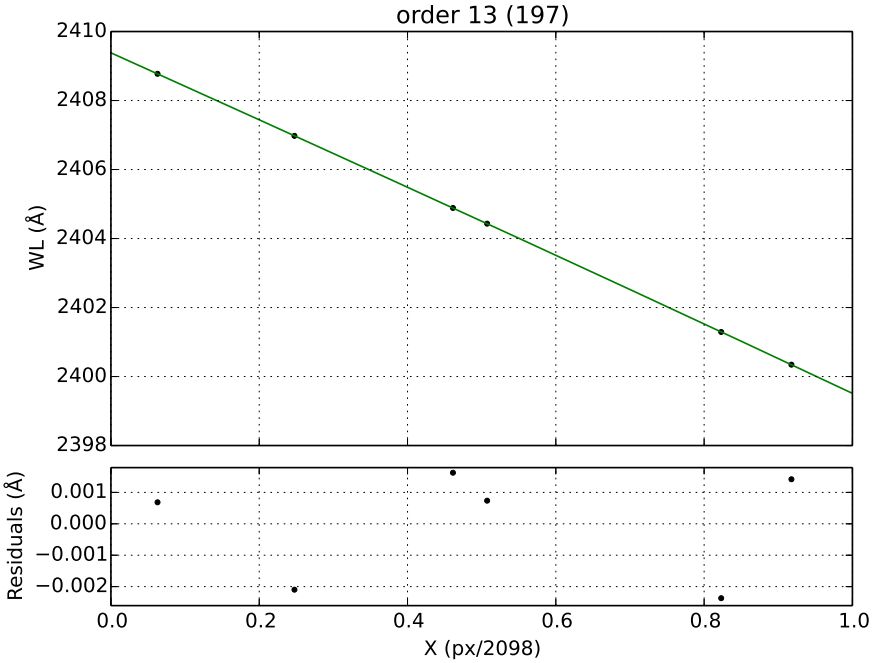

Figure 5.5: Example of a third degree polynomial fit to identified lines in an order. Bottom plot shows the residuals of the fit.

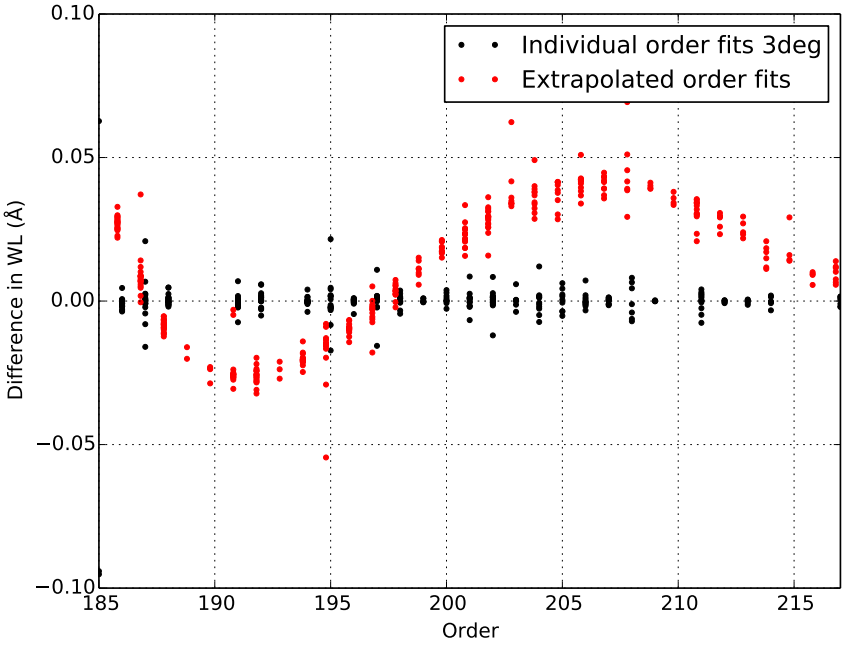

Figure 5.6: Plot showing the first attempt at fitting order coefficients and the resulting wavelengths, sorted by order. Black points show the difference in wavelength between reference lines and wavelengths obtained from polynomials fitted to individual orders. Red points are the difference between references and wavelengths from polynomials calculated from fitted coefficients. Note that the x-axis shows physical order rather than order number on the CCD. Physical order 185 is order 1 on the CCD.

for some other reason. Doing this would also enable much faster processing of any new exposures since it would be possible to determine wavelengths with only a few identified lines in an image as opposed to at least several per order. To enable this polynomials were fit to the coefficients of the individual order polynomials. Both third and fifth order polynomials were fitted since in this case there is 25 data points, so fitting fifth order polynomials is not a problem.

When this was first tried, some quite strange wavelengths resulted. As can be seen in fig. 5.6, the resulting in-order scatter of the resulting wavelengths is on the same level as that of individual order polynomial wavelengths. However, the deviation from the references varies smoothly with order. After quite a while of searching for the reason behind this behaviour it was narrowed down to the constant term of the order polynomials. The fit was simply not working out as well as hoped. The solution that was tried

for a long time was changing the function fitted to the order polynomial coefficients. Higher degree polynomials were tried at first, uneven polynomials up to degree nine were tested and found to not work better than third degree ones. Hybrid versions were also tried, with differing order in the polynomials for different order polynomial coefficients, e.g., third degree for the constant term, linear for the first degree term and higher. This did not turn out better either. Finally, a cubic spline was tried, which worked to a very limited degree. However, due to how spline fitting works, it's hard to draw a line where you are interpolating more than fitting a physically relevant function.

The final solution that turned out to work well was stumbled on very late in the project and was, as is wont to happen, the simplest one. It turns out that since the constant term in the order polynomials span a range of over 400Å, but requires a precision of roughly 0.01Å to be good, it is extremely sensitive to badly fitted order polynomials The solution turned out to be to go over the fits of individual order polynomials and determine which orders were badly determined. There could be different causes for this. The main ones in this instance were identified lines only in a small range on the CCD or misidentified lines. A list of the WL range between lines and the number of identified lines can be found in table 5.1.

As can be seen in table 5.1 orders 5, 9, 26, 31 and 32 can be removed immediately because they have too few identified lines (less than 5) for it to be meaningful to fit a third degree polynomial. In addition to those we can see that order 25 is dubious at best: its data points spans less than half the CCD and there are only five of them. Finally, we also remove order 1 for ending up with a fit that is so drastically different from the normal ones. Both the fits for order 1 and 25 can be seen in fig. 5.7 In these figures you can clearly see that the fitted polynomials are not as straight as the one in the other orders (as exemplified by fig. 5.5). Order 1 has an especially bad fit and order 25's small detector span can be seen as well.

When order 1 and 25 were removed the fit to the linear coefficients became better and consequently the resulting wavelengths became better. This can be seen in fig. 5.9. Fig. 5.9 shows the wavelengths obtained when fitting third degree polynomials to all four coefficients of the individual order polynomials. This is, however, not necessarily justified. When looking at the plots in fig. 5.8 the non-constant coefficients seems to not need, or indeed justify the need for third degree fits. This resulted in trying out a hybrid fit again, simply because it is the simplest fit that can justifiably be made to each of the coefficient series. For the constant coefficient a third degree fit was kept, but the linear coefficient got a linear fit. The cubic and quadratic coefficients got constant values fitted to them. See fig. 5.11 for these fits. The resulting wavelengths can be seen in fig. 5.10.

Table 5.1: Table showing the x-coordinate span of identified spectral lines in *fe05201* along with number of fitted profiles and identified lines in each order. The total span of the CCD is 2098 pixels and the useful span is roughly 2040 pixels.

Order	Span (pixels)	No. of fit profiles	No. of ID:d lines
1 (185)	1319	14	6
2 (186)	1503	23	5
3 (187)	1622	22	11
4 (188)	1354	24	7
5 (189)	607	19	2
6 (190)	1715	20	8
7 (191)	1166	21	7
8 (192)	1660	24	8
9 (193)	1115	21	3
10 (194)	1318	21	6
11 (195)	1773	19	15
12 (196)	1594	18	9
13 (197)	1794	18	6
14 (198)	1597	19	7
15 (199)	1358	12	7
16 (200)	1628	10	8
17 (201)	1888	17	13
18 (202)	1767	20	15
19 (203)	1498	9	8
20 (204)	1368	15	10
21 (205)	1776	9	9
22 (206)	1491	12	12
23 (207)	1885	10	10
24 (208)	1419	8	6
25 (209)	984	5	5
26 (210)	1742	4	4
27 (211)	1671	13	13
28 (212)	1940	6	6
29 (213)	1812	6	5
30 (214)	1478	6	6
31 (215)	458	4	4
32 (216)	1131	4	4
33 (217)	1860	7	7

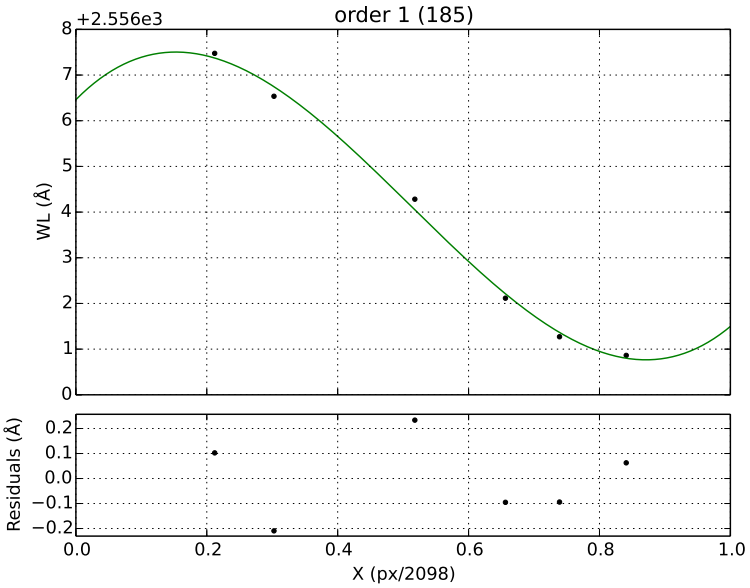

(a) Polynomial fit of order one. Note how different this is from fig. 5.5, an example of a typical fit.

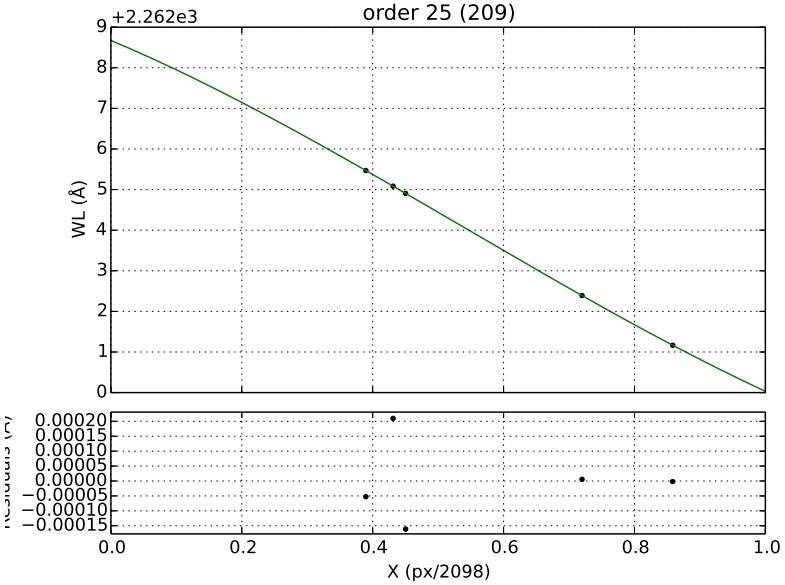

(b) Polynomial fit of order 25. Note how it bends downwards at the start and upwards at the end like a less extreme version of order 1.

Figure 5.7: The individual order polynomial fits for orders 1 and 25. These were both removed from coefficient fitting for likely having misidentified lines making the polynomials useless.

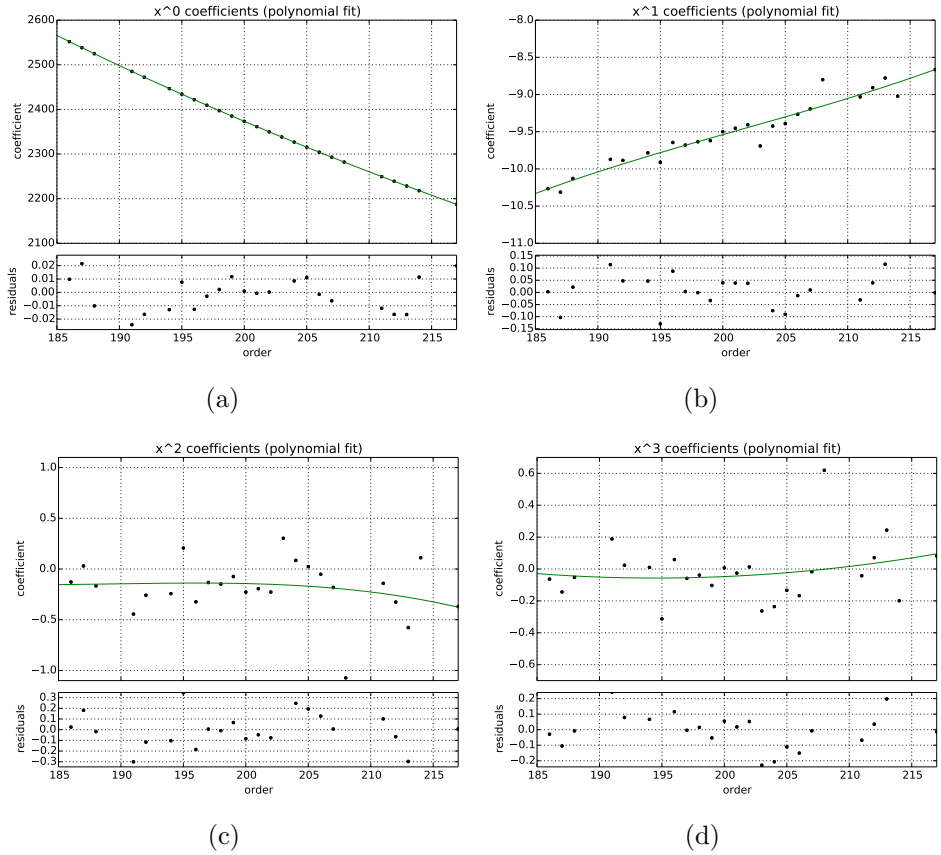

Figure 5.8: Four plots showing the fits to the four coefficients of the various individual order polynomials. All plots also show the residuals of the fit. These show third degree polynomials fitted to each data set. These fits lead to the wavelengths in the red points in fig. 5.9.

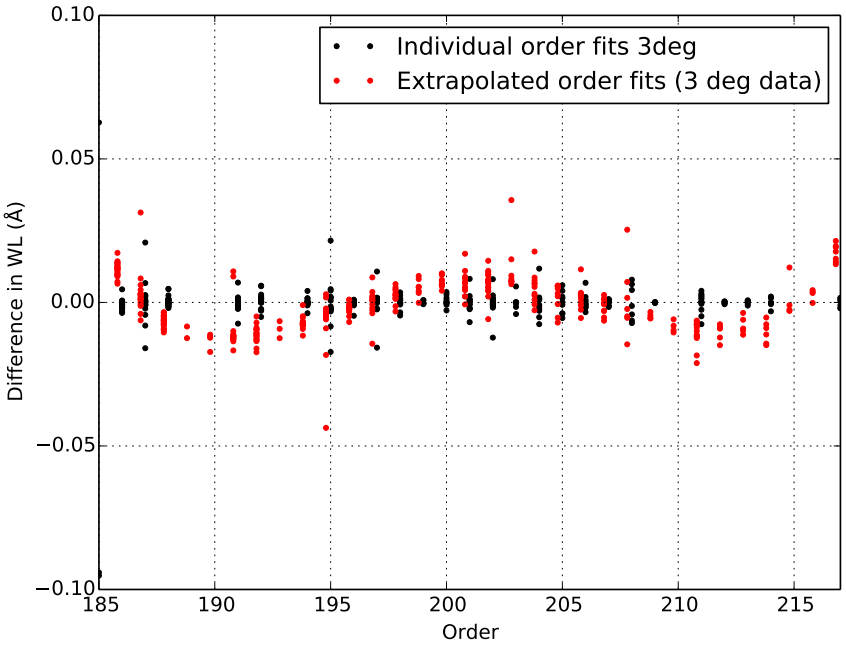

Figure 5.9: The same plot as fig. 5.6 but with orders 1 (185) and 25 (209) removed from the fit of the linear coefficients in each third degree polynomial (see fig. 5.8). Note that the red points are offset slightly in x-position from the black ones to enable comparisons between them.

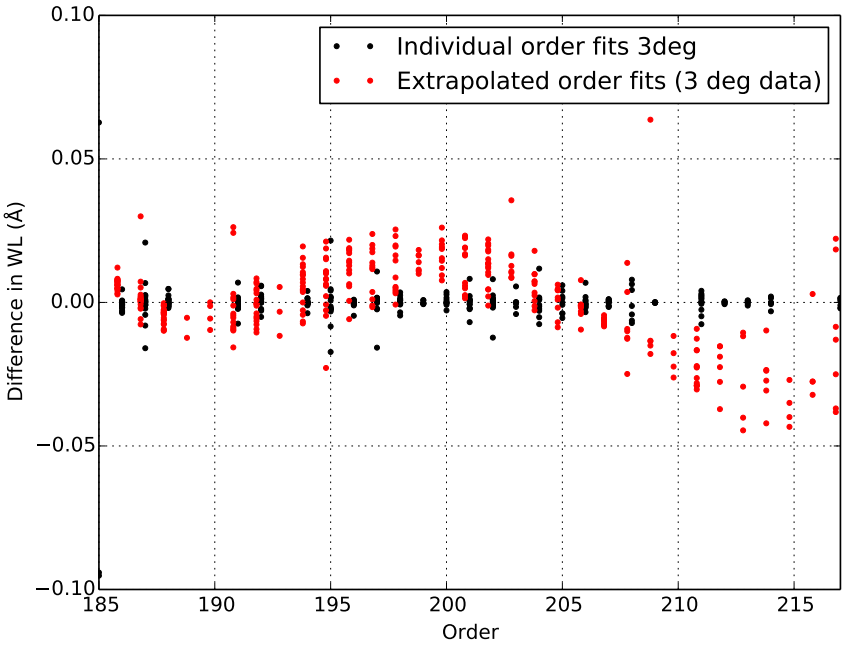

Figure 5.10: The same plot as fig. 5.6 but with orders 1 (185) and 25 (209) removed from the fit of the linear coefficients in each third degree polynomial. Note that the red points are offset slightly in x-position from the black ones to enable comparisons between them.

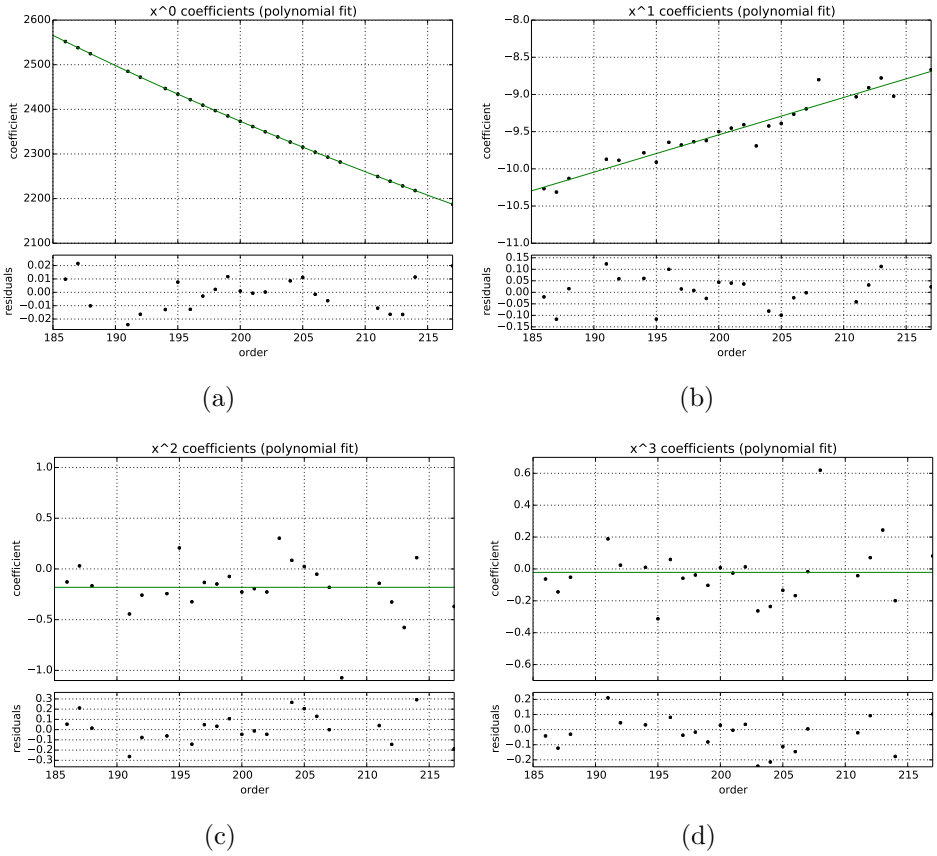

Figure 5.11: Four plots showing the fits to the four coefficients of the various individual order polynomials. All plots also show the residuals of the fit. These show a third degree fit in subfigure a, a linear fit in subfigure b, and a constant fitted in subfigures c and d (see fig. 5.11). These fits lead to the wavelengths in the red points in fig. 5.10.

Chapter 6

Discussion and Summary

This section will briefly discuss the results of both the improvements made to LOVES and the results of the wavelength determinations.

6.1 LOVES Instrumentation Progress

As of the end of this project, LOVES is functional but very cumbersome to use. There is still work that needs to be done to get the instrument into a state where it can reliably do good science. Nevertheless, this project has taken big steps in the right direction. The most important step towards a full-fledged LOVES is to refine and streamline the data reduction process. Currently, it is very hands-on and the instrument requires quite a bit of knowledge of how it works to be used. E.g., to place a specific spectral line on the detector an intimate knowledge of how the OSG movement relates to the detector is needed.

However, compared to LOVES' state at the beginning of the project some major improvements have taken place. The optics are aligned and focussed and the OSG rotation counter has been normalised. Software for conversion and handling of the output files from OIUSBCCD now exist and are usable. Refinement of the software would be something of a luxury for the future but would undoubtedly be a good thing. Additionally, testing LOVES in the UV, similarly to how this project tested it at around 2400Å should be a priority for any future work.

6.2 Wavelengths

This project has determined wavelengths for 459 lines of mainly Fe I and Fe II in the wavelength region 2170 - 2570 Å using secondary iron reference lines. Of these, 391 have been determined using internal order references. The remaining 68 were in orders where there were not enough internal order references and are therefore determined only through interpolated order

polynomials. These values are all listed in the tables of App. A. Note that it is entirely possible that a few of these lines are entirely new, unmeasured, iron lines. There has been no investigation as to whether they are new or not due to a lack of time at the end of the project.

Figs. 5.9 and 5.10 contain visualisations of these wavelengths and their relation to the reference lines. Fig. 5.9 contains the wavelengths resulting from fitting a third degree polynomial to each set of individual order coefficients while fig. 5.9 contains the results of the hybrid approach, as described in section 5.4. As can be clearly seen, they are a bit different. Essentially, the third degree fit wavelengths are better, but it is not obvious if it is motivated to use third degree fits for all coefficients. The fairly large spread in the data points in fig. 5.8a and 5.8b illustrates this. It is not obvious that a third degree fit should be used, based on the physics of the set-up either. The true relationship between position and wavelength is quite complicated and depends on several variables that are simply not available at the required precision or simply not available at all, e.g., the distance from the OSG to the detector or the incident angle of the light on the echelle grating.

The hybrid scheme described at the end of section 5.4 is the simplest possible way to recreate reasonable wavelength values. This means that it is generally preferred over the more intricate third degree approach. As can be seen when comparing fig 5.9 and fig 5.10 the third degree approach recreates the references better. However, this is unsurprising, given that a higher degree fit will always be better. The main difference between the two schemes is that in the hybrid scheme the in-order scatter of the wavelengths is about twice as large as the third degree scheme. Additionally, the hybrid scheme gets worse faster with increasing order (decreasing wavelength). Both approaches show a systematic variation of the wavelength compared to the references. This variation mainly comes from an inaccurate fit of the constant terms in the order polynomials while the in-order scatter mainly comes from the higher order coefficient fits. Improving the wavelengths is likely possible with a careful investigation of the reference line identifications. An addition of more identified lines would likely improve the wavelengths as well. However, the addition of more identified lines would not necessarily be of use for this project since it endeavours to show that it is possible to obtain consistent wavelengths using only a smaller number of lines.

Bibliography

Brandt J. C. et al., 1999, The Astronomical Journal, 117, 1505

Edlén B., 1963, Reports on Progress in Physics, 26, 181

Johansson S., 1978, Physica Scripta, 18, 217

Leckrone D. S., Proffitt C. R., Wahlgren G. M., Johansson S. G., Brage T., 1999, The Astronomical Journal, 117, 1454

Moore C. E., 1970, Nat. Stand. Ref. Data Ser., NSRDS-NBS 3 (Sect. 3)

Moore C. E., 1976, Nat. Stand. Ref. Data Ser., NSRDS-NBS 3 (Sect. 7)

Nave G., Johansson S., 2013, The Astrophysical Journal Supplement Series, 204, 1

Richter P., de Boer K. S., Werner K., Rauch T., 2015, Astronomy & Astrophysics, 584, L6

Thorne A., Litzén U., Johansson S., 1999, Spectrophysics. Springer

Appendices

Appendix A

Wavelength Tables

This appendix contains a complete table of reference lines and identified lines in fe05201. All the tables are structured the same way: Column "Ion" list the ion of the identified line as taken from Sveneric's compendium. Lines marked with a "?" are lines that lack an ion identification in the compendium. Column "ID'd wl" lists the identified wavelength along with an "H" or a "P" which indicates who made the identification of that particular line. "H" Markers are for Hampus Nilsson while "P" markers are for Petter Thorén. Column "Ind. Fit WL" lists the wavelength obtained for that line when fitting third degree polynomials to individual orders, as described in section 5.4 above. Column "3 Deg. WL" lists wavelengths obtained for that line when using third degree polynomials for all coefficients, similar to what can be seen in fig. 5.9. Column "Hybrid WL" is similar, listing wavelengths obtained for that line when using the hybrid scheme, as seen in fig. 5.10. Please note that all wavelengths are vacuum wavelengths, because LOVES is a vacuum instrument, despite being above 2000Å. After each of the calculated wavelength columns there is also a column listing the difference between the identified line wavelength and the calculated wavelength.

Table A.1: Wavelength table for order 1(185).

Ion	ID'd λ_{vac}		Ind. Fit λ_{vac}	Δ λ_{vac}	3 Deg. λ_{vac}	Δ λ_{vac}	Hybrid λ_{vac}	Δ λ_{vac}
			2563.4258		2564.5223		2564.5257	
Fe II	2563.4755	H	2563.3730	0.1025	2563.4521	0.0234	2563.4580	0.0175
Fe II	2562.5356	H	2562.7450	-0.2094	2562.5087	0.0269	2562.5166	0.0190
			2562.3162		2562.0696		2562.0783	
			2560.6250		2560.6861		2560.6967	
			2560.4166		2560.5296		2560.5404	
Fe II	2560.2825	H	2560.0490	0.2335	2560.2549	0.0276	2560.2660	0.0165
			2559.5742		2559.8982		2559.9098	
			2559.3725		2559.7446		2559.7563	
?	2558.1156	H	2558.2108	-0.0952	2558.7957	-0.6801	2558.8081	-0.6925
Fe I	2557.2706	H	2557.3647	-0.0941	2557.9210	-0.6504	2557.9340	-0.6634
			2557.0603		2557.4817		2557.4950	
Fe I	2556.8629	H	2556.8002	0.0627	2556.8379	0.0250	2556.8514	0.0115
			2556.7856		2556.2801		2556.2938	
			2557.2090		2555.4308		2555.4447	

Table A.2: Wavelength table for order 2(186).

Ion	ID'd λ_{vac}		Ind. Fit λ_{vac}	Δ λ_{vac}	3 Deg. λ_{vac}	Δ λ_{vac}	Hybrid λ_{vac}	Δ λ_{vac}
			2551.3971		2551.3871		2551.3881	
Fe I	2551.0933	P	2551.0969	-0.0036	2551.0868	0.0065	2551.0883	0.0050
Fe II	2550.6832	P	2550.6864	-0.0032	2550.6760	0.0072	2550.6783	0.0049
Fe II	2550.1515	P	2550.1533	-0.0018	2550.1424	0.0091	2550.1455	0.0060
Fe II	2550.0275	P	2550.0291	-0.0016	2550.0181	0.0094	2550.0213	0.0062
Fe II	2549.6133	H	2549.6133	0.0000	2549.6020	0.0113	2549.6058	0.0075
Fe II	2548.7442	P	2548.7445	-0.0003	2548.7324	0.0118	2548.7371	0.0071
Fe II	2548.5893	P	2548.5893	0.0000	2548.5770	0.0123	2548.5818	0.0075
Fe II	2548.3252	P	2548.3281	-0.0029	2548.3156	0.0096	2548.3205	0.0047
Fe I	2548.1002	P	2548.0956	0.0046	2548.0829	0.0173	2548.0881	0.0121
Fe II	2547.3384	P	2547.3381	0.0003	2547.3247	0.0137	2547.3303	0.0081
Fe I	2546.8675	P	2546.8676	-0.0001	2546.8539	0.0136	2546.8597	0.0078
Fe II	2546.6701	P	2546.6711	-0.0010	2546.6573	0.0128	2546.6632	0.0069
	2546.4420	P	2546.4439	-0.0019	2546.4301	0.0119	2546.4360	0.0060
Fe I	2545.9784	H	2545.9781	0.0003	2545.9641	0.0143	2545.9702	0.0082
Fe II	2545.2199	P	2545.2217	-0.0018	2545.2077	0.0122	2545.2140	0.0059
Fe II			2544.9756		2544.9616		2544.9679	
?	2544.7065	H	2544.7074	-0.0009	2544.6935	0.0130	2544.6998	0.0067
Fe I	2543.9224	H	2543.9217	0.0007	2543.9083	0.0141	2543.9149	0.0075
Fe II	2543.0804	P	2543.0811	-0.0007	2543.0688	0.0116	2543.0755	0.0049
Fe II	2542.7361	P	2542.7369	-0.0008	2542.7252	0.0109	2542.7320	0.0041
Fe I	2542.1014	H	2542.1015	-0.0001	2542.0912	0.0102	2542.0982	0.0032
Fe II	2541.8358	P	2541.8355	0.0003	2541.8259	0.0099	2541.8330	0.0028

Table A.3: Wavelength table for order 3(187).

Ion	ID'd λ_{vac}		Ind. Fit λ_{vac}	$\Delta\ \lambda_{vac}$	3 Deg. λ_{vac}	$\Delta\ \lambda_{vac}$	Hybrid λ_{vac}	$\Delta\ \lambda_{vac}$
			2537.4760		2537.4612		2537.4620	
Fe II	2537.1747	H	2537.1790	-0.0043	2537.1664	0.0083	2537.1675	0.0072
Fe II	2536.8453	H	2536.8244	0.0209	2536.8140	0.0313	2536.8153	0.0300
Fe II	2536.6726	H	2536.6886	-0.0160	2536.6788	-0.0062	2536.6803	-0.0077
Fe I	2535.6071	H	2535.6093	-0.0022	2535.6040	0.0031	2535.6058	0.0013
?	2535.1317	P	2535.1398	-0.0081	2535.1357	-0.0040	2535.1375	-0.0058
Fe II	2534.4187	H	2534.4187	0.0000	2534.4158	0.0029	2534.4176	0.0011
Fe I	2533.8042	H	2533.8022	0.0020	2533.7998	0.0044	2533.8015	0.0027
Fe II	2533.6274	H	2533.6271	0.0003	2533.6248	0.0026	2533.6264	0.0010
?			2532.3736		2532.3713		2532.3725	
Fe II	2531.8712	P	2531.8708	0.0004	2531.8684	0.0028	2531.8695	0.0017
?	2531.4306	P	2531.4310	-0.0004	2531.4286	0.0020	2531.4295	0.0011
?			2531.1964		2531.1940		2531.1949	
?	2530.6913	H	2530.6922	-0.0009	2530.6900	0.0013	2530.6908	0.0005
Fe II	2530.1078	P	2530.1087	-0.0009	2530.1069	0.0009	2530.1077	0.0001
Fe II	2529.8354	H	2529.8353	0.0001	2529.8339	0.0015	2529.8347	0.0007
Fe II	2529.5481	H	2529.5490	-0.0009	2529.5481	0.0000	2529.5488	-0.0007
Fe I	2529.3076	P	2529.3052	0.0024	2529.3047	0.0029	2529.3055	0.0021
Fe I	2529.1351	H	2529.1341	0.0010	2529.1340	0.0011	2529.1348	0.0003
Fe I	2528.8775	P	2528.8708	0.0067	2528.8714	0.0061	2528.8723	0.0052
?	2528.5079	P	2528.5072	0.0007	2528.5091	-0.0012	2528.5101	-0.0022
Fe II	2528.1710	P	2528.1684	0.0026	2528.1717	-0.0007	2528.1728	-0.0018

Table A.4: Wavelength table for order 4(188).

Ion	ID'd λ_{vac}		Ind. Fit λ_{vac}	Δ λ_{vac}	3 Deg. λ_{vac}	Δ λ_{vac}	Hybrid λ_{vac}	Δ λ_{vac}
Fe I	2524.2925	H	2524.2928	-0.0003	2524.3020	-0.0095	2524.3022	-0.0097
Si I	2524.1074	P	2524.1076	-0.0002	2524.1165	-0.0091	2524.1167	-0.0093
Fe I	2523.6611	H	2523.6604	0.0007	2523.6685	-0.0074	2523.6688	-0.0077
Fe II	2523.4416	P	2523.4435	-0.0019	2523.4512	-0.0096	2523.4515	-0.0099
Fe I	2523.1380	P	2523.1368	0.0012	2523.1440	-0.0060	2523.1442	-0.0062
Fe I	2522.8497	H	2522.8502	-0.0005	2522.8570	-0.0073	2522.8571	-0.0074
			2522.5015		2522.5078		2522.5078	
Fe II	2522.1965	P	2522.1962	0.0003	2522.2021	-0.0056	2522.2019	-0.0054
Fe II	2521.0917	P	2521.0914	0.0003	2521.0964	-0.0047	2521.0954	-0.0037
Fe II	2520.6724	P	2520.6727	-0.0003	2520.6774	-0.0050	2520.6761	-0.0037
Fe II	2520.2625	P	2520.2638	-0.0013	2520.2684	-0.0059	2520.2667	-0.0042
Fe I	2519.6294	H	2519.6283	0.0011	2519.6329	-0.0035	2519.6306	-0.0012
?	2519.2018	P	2519.2005	0.0013	2519.2052	-0.0034	2519.2026	-0.0008
Fe II	2519.0472	H	2519.0487	-0.0015	2519.0535	-0.0063	2519.0508	-0.0036
Fe II	2518.5349	P	2518.5360	-0.0011	2518.5411	-0.0062	2518.5379	-0.0030
Fe I	2518.1017	H	2518.1008	0.0009	2518.1063	-0.0046	2518.1028	-0.0011
Fe II	2517.6612	H	2517.6616	-0.0004	2517.6676	-0.0064	2517.6638	-0.0026
Fe II	2517.1321	P	2517.1297	0.0024	2517.1365	-0.0044	2517.1324	-0.0003
?	2516.8817	P	2516.8822	-0.0005	2516.8895	-0.0078	2516.8853	-0.0036
Fe I	2516.5709	P	2516.5705	0.0004	2516.5784	-0.0075	2516.5741	-0.0032
			2516.1090		2516.1179		2516.1135	
Fe II	2515.9058	P	2515.9069	-0.0011	2515.9163	-0.0105	2515.9119	-0.0061
Fe II	2515.1195	P	2515.1148	0.0047	2515.1263	-0.0068	2515.1221	-0.0026
Fe I	2514.7095	P	2514.7048	0.0047	2514.7177	-0.0082	2514.7136	-0.0041

Table A.5: Wavelength table for order 5(189).

Ion	ID'd λ_{vac}		Ind. Fit λ_{vac}	Δ λ_{vac}	3 Deg. λ_{vac}	Δ λ_{vac}	Hybrid λ_{vac}	Δ λ_{vac}
Fe I	2510.8351	H	n/a		2510.8475	-0.0124	2510.8474	-0.0123
			n/a		2509.8751		2509.8744	
			n/a		2509.1357		2509.1343	
			n/a		2508.3512		2508.3488	
Fe I	2507.9003	H	n/a		2507.9087	-0.0084	2507.9056	-0.0053
			n/a		2507.0379		2507.0336	
			n/a		2506.8047		2506.8001	
			n/a		2506.5772		2506.5722	
			n/a		2506.4361		2506.4309	
			n/a		2506.2827		2506.2773	
			n/a		2506.1042		2506.0986	
			n/a		2505.6393		2505.6330	
			n/a		2505.4713		2505.4648	
			n/a		2503.8851		2503.8769	
			n/a		2503.3390		2503.3304	
			n/a		2502.4048		2502.3960	
			n/a		2502.0060		2501.9973	
			n/a		2501.7005		2501.6919	
			n/a		2501.3329		2501.3245	

Table A.6: Wavelength table for order 6(190).

Ion	ID'd λ_{vac}		Ind. Fit λ_{vac}	Δ λ_{vac}	3 Deg. λ_{vac}	Δ λ_{vac}	Hybrid λ_{vac}	Δ λ_{vac}
			n/a		2497.8357		2497.8355	
			n/a		2497.0044		2497.0034	
Fe I	2496.5338	H	n/a		2496.5451	-0.0113	2496.5434	-0.0096
			n/a		2495.8788		2495.8761	
			n/a		2494.2619		2494.2563	
			n/a		2494.0103		2494.0041	
			n/a		2493.8886		2493.8822	
			n/a		2493.7640		2493.7573	
			n/a		2492.9032		2492.8949	
			n/a		2492.3721		2492.3629	
			n/a		2492.1595		2492.1499	
			n/a		2491.9921		2491.9823	
			n/a		2491.4108		2491.4001	
Fe II	2491.1550	H	n/a		2491.1673	-0.0123	2491.1562	-0.0012
			n/a		2490.8717		2490.8603	
Fe I	2490.6443	H	n/a		2490.6615	-0.0172	2490.6499	-0.0056
			n/a		2489.8430		2489.8308	
			n/a		2489.5000		2489.4876	
			n/a		2488.9575		2488.9451	
Fe I	2488.1428	H	n/a		2488.1548	-0.0120	2488.1428	0.0000

Table A.7: Wavelength table for order 7(191).

Ion	ID'd λ_{vac}		Ind. Fit λ_{vac}	Δ λ_{vac}	3 Deg. λ_{vac}	Δ λ_{vac}	Hybrid λ_{vac}	Δ λ_{vac}
			2484.7037		2484.7241		2484.7237	
			2484.4392		2484.4573		2484.4566	
			2484.1868		2484.2030		2484.2020	
Fe I	2484.1875	H	2484.1880	-0.0005	2484.2042	-0.0167	2484.2032	-0.0157
Fe I	2483.5334	H	2483.5322	0.0012	2483.5450	-0.0116	2483.5429	-0.0095
Fe I	2483.2714	H	2483.2719	-0.0005	2483.2838	-0.0124	2483.2812	-0.0098
Fe II	2482.8670	P	2482.8678	-0.0008	2482.8788	-0.0118	2482.8754	-0.0084
Fe II	2482.6576	P	2482.6598	-0.0022	2482.6704	-0.0128	2482.6665	-0.0089
Fe II	2482.1173	P	2482.1189	-0.0016	2482.1293	-0.0120	2482.1242	-0.0069
Fe II	2481.0497	P	2481.0516	-0.0019	2481.0626	-0.0129	2481.0550	-0.0053
Fe II	2480.9516	P	2480.9529	-0.0013	2480.9640	-0.0124	2480.9562	-0.0046
Fe II	2480.1576	H	2480.1594	-0.0018	2480.1711	-0.0135	2480.1615	-0.0039
Fe II	2479.7764	H	2479.7761	0.0003	2479.7880	-0.0116	2479.7775	-0.0011
Fe I	2479.4804	H	2479.4785	0.0019	2479.4904	-0.0100	2479.4793	0.0011
Fe II	2478.5722	H	2478.5728	-0.0006	2478.5833	-0.0111	2478.5705	0.0017
			2477.9124		2477.9203		2477.9064	
Fe II	2477.3435	P	2477.3508	-0.0073	2477.3551	-0.0116	2477.3405	0.0030
Fe II	2476.6796	P	2476.6726	0.0070	2476.6706	0.0090	2476.6554	0.0242
			2476.4895		2476.4853		2476.4700	
?	2476.0548	P	2476.0541	0.0007	2476.0440	0.0108	2476.0286	0.0262
			2475.5725		2475.5543	-2475.5543	2475.5389	

Table A.8: Wavelength table for order 8(192).

Ion	ID'd λ_{vac}		Ind. Fit λ_{vac}	Δ λ_{vac}	3 Deg. λ_{vac}	Δ λ_{vac}	Hybrid λ_{vac}	Δ λ_{vac}
Fe II	2471.2759	P	2471.2744	0.0015	2471.2876	-0.0117	2471.2864	-0.0105
	2470.9654	P	2470.9626	0.0028	2470.9749	-0.0095	2470.9731	-0.0077
Fe II	2470.6694	H	2470.6694	0.0000	2470.6811	-0.0117	2470.6787	-0.0093
Fe II	2470.4091	P	2470.4073	0.0018	2470.4186	-0.0095	2470.4156	-0.0065
	2469.7175	P	2469.7117	0.0058	2469.7224	-0.0049	2469.7178	-0.0003
Fe I	2468.8798	H	2468.8797	0.0001	2468.8903	-0.0105	2468.8836	-0.0038
Fe II	2468.5006	P	2468.5031	-0.0025	2468.5139	-0.0133	2468.5062	-0.0056
Fe II	2468.2961	P	2468.2939	0.0022	2468.3049	-0.0088	2468.2966	-0.0005
			2467.9845		2467.9957		2467.9866	
Fe II	2467.7335	H	2467.7330	0.0005	2467.7444	-0.0109	2467.7346	-0.0011
Fe I	2468.5686	P	2467.5682	1.0004	2467.5797	0.9889	2467.5695	0.9991
Fe II	2466.8194	H	2466.8183	0.0011	2466.8306	-0.0112	2466.8185	0.0009
Fe II	2466.6714	H	2466.6764	-0.0050	2466.6888	-0.0174	2466.6763	-0.0049
Fe II			2466.4978		2466.5104		2466.4975	
Fe II	2465.9136	H	2465.9077	0.0059	2465.9207	-0.0071	2465.9065	0.0071
Fe I	2465.1493	H	2465.1521	-0.0028	2465.1654	-0.0161	2465.1497	-0.0004
Fe II	2464.9054	P	2464.9050	0.0004	2464.9183	-0.0129	2464.9022	0.0032
			2464.1963		2464.2091		2464.1921	
Fe II	2464.0098	P	2464.0096	0.0002	2464.0223	-0.0125	2464.0051	0.0047
Fe II	2463.7304	P	2463.7290	0.0014	2463.7412	-0.0108	2463.7238	0.0066
Fe II	2463.2815	P	2463.2837	-0.0022	2463.2950	-0.0135	2463.2773	0.0042
			2462.9552		2462.9656		2462.9479	
Fe I	2462.6473	H	2462.6472	0.0001	2462.6566	-0.0093	2462.6389	0.0084
			2462.3166		2462.3248		2462.3073	

Table A.9: Wavelength table for order 9(193).

Ion	ID'd λ_{vac}		Ind. Fit λ_{vac}	Δ λ_{vac}	3 Deg. λ_{vac}	Δ λ_{vac}	Hybrid λ_{vac}	Δ λ_{vac}
			n/a		2458.9854		2458.9849	
Fe II	2458.7838	H	n/a		2458.7963	-0.0125	2458.7954	-0.0116
			n/a		2458.5695		2458.5683	
Fe I	2457.5968	H	n/a		2457.6033	-0.0065	2457.6000	-0.0032
			n/a		2457.3484		2457.3445	
			n/a		2457.1110		2457.1065	
			n/a		2456.9742		2456.9693	
			n/a		2456.1954		2456.1884	
			n/a		2455.9081		2455.9003	
			n/a		2455.7103		2455.7018	
			n/a		2455.5789		2455.5701	
			n/a		2454.5887		2454.5770	
			n/a		2453.9851		2453.9718	
			n/a		2453.7975		2453.7837	
Fe II	2453.4760	H	n/a		2453.4852	-0.0092	2453.4706	0.0054
			n/a		2453.1618		2453.1465	
			n/a		2452.4947		2452.4780	
			n/a		2452.1608		2452.1434	
			n/a		2451.6850		2451.6669	
			n/a		2451.2279		2451.2092	
			n/a		2449.5987		2449.5795	

Table A.10: Wavelength table for order 10(194).

Ion	ID'd λ_{vac}		Ind. Fit λ_{vac}	$\Delta\ \lambda_{vac}$	3 Deg. λ_{vac}	$\Delta\ \lambda_{vac}$	Hybrid λ_{vac}	$\Delta\ \lambda_{vac}$
			2446.1087		2446.1194		2446.1185	
Fe II	2445.7957	P	2445.7942	0.0015	2445.8038	-0.0081	2445.8024	-0.0067
Fe II	2445.5732	H	2445.5735	-0.0003	2445.5824	-0.0092	2445.5805	-0.0073
Fe II	2445.1067	H	2445.1061	0.0006	2445.1140	-0.0073	2445.1110	-0.0043
Fe II	2444.5154	H	2444.5157	-0.0003	2444.5227	-0.0073	2444.5182	-0.0028
			2444.3002		2444.3069		2444.3018	
Fe II	2443.7101	P	2443.7105	-0.0004	2443.7169	-0.0068	2443.7101	0.0000
Fe II	2442.5685	H	2442.5685	0.0000	2442.5751	-0.0066	2442.5649	0.0036
Fe II	2442.3760	P	2442.3745	0.0015	2442.3812	-0.0052	2442.3704	0.0056
Fe II	2442.1327	P	2442.1332	-0.0005	2442.1400	-0.0073	2442.1285	0.0042
			2441.6368		2441.6439		2441.6310	
Fe II	2441.1297	P	2441.1297	0.0000	2441.1372	-0.0075	2441.1228	0.0069
Fe II	2440.5866	P	2440.5865	0.0001	2440.5943	-0.0077	2440.5785	0.0081
Fe II	2440.4246	P	2440.4283	-0.0037	2440.4362	-0.0116	2440.4200	0.0046
Fe II	2440.1097	P	2440.1092	0.0005	2440.1172	-0.0075	2440.1002	0.0095
Fe I	2439.7450	H	2439.7449	0.0001	2439.7529	-0.0079	2439.7352	0.0098
Fe II	2439.3014	H	2439.3015	-0.0001	2439.3095	-0.0081	2439.2909	0.0105
Fe I	2438.1826	P	2438.1832	-0.0006	2438.1903	-0.0077	2438.1702	0.0124
Fe II	2437.6521	P	2437.6531	-0.0010	2437.6592	-0.0071	2437.6388	0.0133
Fe II	2437.2038	P	2437.1998	0.0040	2437.2047	-0.0009	2437.1843	0.0195
Fe II	2436.9965	P	2436.9970	-0.0005	2437.0013	-0.0048	2436.9810	0.0155

Table A.11: Wavelength table for order 11(195).

Ion	ID'd λ_{vac}		Ind. Fit λ_{vac}	Δ λ_{vac}	3 Deg. λ_{vac}	Δ λ_{vac}	Hybrid λ_{vac}	Δ λ_{vac}
Fe II	2432.8731	H	2432.8745	-0.0014	2432.8781	-0.0050	2432.8759	-0.0028
Fe II	2432.2612	H	2432.2595	0.0017	2432.2657	-0.0045	2432.2619	-0.0007
Fe II	2432.0322	P	2432.0345	-0.0023	2432.0412	-0.0090	2432.0369	-0.0047
			2430.8671		2430.8738		2430.8661	
Fe II	2430.0783	H	2430.0776	0.0007	2430.0827	-0.0044	2430.0725	0.0058
Fe II	2429.8608	H	2429.8591	0.0017	2429.8637	-0.0029	2429.8528	0.0080
Fe II	2429.3865	H	2429.3891	-0.0026	2429.3924	-0.0059	2429.3801	0.0064
Fe II	2429.1540	H	2429.1560	-0.0020	2429.1587	-0.0047	2429.1457	0.0083
Fe II	2429.0361	H	2429.0319	0.0042	2429.0344	0.0017	2429.0210	0.0151
			2429.0348		2429.0373		2429.0240	
Fe II	2428.8003	H	2428.8023	-0.0020	2428.8042	-0.0039	2428.7903	0.0100
Fe II	2428.6412	P	2428.6435	-0.0023	2428.6451	-0.0039	2428.6307	0.0105
Fe II	2428.3638	H	2428.3669	-0.0031	2428.3681	-0.0043	2428.3529	0.0109
			2427.4967		2427.4977		2427.4803	
Fe II	2427.0548	H	2427.0502	0.0046	2427.0520	0.0028	2427.0336	0.0212
Fe II	2426.0778	H	2426.0758	0.0020	2426.0822	-0.0044	2426.0622	0.0156
Fe II	2425.6379	H	2425.6462	-0.0083	2425.6562	-0.0183	2425.6357	0.0022
Fe II	2424.5929	H	2424.5713	0.0216	2424.5950	-0.0021	2424.5741	0.0188
Fe II	2424.3899	H	2424.4071	-0.0172	2424.4336	-0.0437	2424.4127	-0.0228

Table A.12: Wavelength table for order 12(196).

Ion	ID'd λ_{vac}		Ind. Fit λ_{vac}	Δ λ_{vac}	3 Deg. λ_{vac}	Δ λ_{vac}	Hybrid λ_{vac}	Δ λ_{vac}
Fe II	2421.0408	P	2421.0398	0.0010	2421.0476	-0.0068	2421.0466	-0.0058
Fe II	2419.9884	H	2419.9886	-0.0002	2419.9911	-0.0027	2419.9879	0.0005
Fe II	2418.6651	P	2418.6656	-0.0005	2418.6656	-0.0005	2418.6587	0.0064
			2418.0019		2418.0019		2417.9930	
Fe II	2417.8707	H	2417.8699	0.0008	2417.8699	0.0008	2417.8606	0.0101
			2417.6953		2417.6954		2417.6856	
Fe II	2417.4979	P	2417.5025	-0.0046	2417.5027	-0.0048	2417.4923	0.0056
			2416.5778		2416.5790		2416.5658	
Fe II	2416.4455	H	2416.4465	-0.0010	2416.4478	-0.0023	2416.4342	0.0113
Fe II	2416.0802	P	2416.0803	-0.0001	2416.0820	-0.0018	2416.0674	0.0128
Fe II	2415.3613	H	2415.3608	0.0005	2415.3633	-0.0020	2415.3468	0.0145
	2415.0671	H	2415.0677	-0.0006	2415.0704	-0.0033	2415.0532	0.0139
			2414.2035		2414.2062		2414.1872	
Fe II	2413.9934	H	2413.9931	0.0003	2413.9956	-0.0022	2413.9762	0.0172
Fe II	2413.6719	H	2413.6715	0.0004	2413.6737	-0.0018	2413.6538	0.0181
Fe II	2413.4960	P	2413.4957	0.0003	2413.4975	-0.0015	2413.4775	0.0185
Fe II	2413.3104	H	2413.3103	0.0001	2413.3118	-0.0014	2413.2915	0.0189
Fe II	2412.4377	H	2412.4380	-0.0003	2412.4367	0.0010	2412.4159	0.0218

Table A.13: Wavelength table for order 13(197).

Ion	ID'd λ_{vac}		Ind. Fit λ_{vac}	$\Delta\ \lambda_{vac}$	3 Deg. λ_{vac}	$\Delta\ \lambda_{vac}$	Hybrid λ_{vac}	$\Delta\ \lambda_{vac}$
Fe II	2408.7747	H	2408.7740	0.0007	2408.7766	-0.0019	2408.7757	-0.0010
Fe II	2408.6485	P	2408.6487	-0.0002	2408.6512	-0.0027	2408.6501	-0.0016
Fe II	2407.7671	P	2407.7563	0.0108	2407.7584	0.0087	2407.7555	0.0116
			2407.2284		2407.2302		2407.2260	
Fe II	2406.9762	H	2406.9783	-0.0021	2406.9800	-0.0038	2406.9751	0.0011
			2405.4223		2405.4231		2405.4138	
Fe II	2404.8858	H	2404.8842	0.0016	2404.8846	0.0012	2404.8737	0.0121
Fe II	2404.4310	H	2404.4303	0.0007	2404.4304	0.0006	2404.4182	0.0128
Fe II	2404.0611	P	2404.0606	0.0005	2404.0605	0.0006	2404.0472	0.0139
?	2403.3379	P	2403.3362	0.0017	2403.3356	0.0023	2403.3204	0.0175
			2402.6258		2402.6248		2402.6079	
			2402.4463		2402.4452		2402.4279	
Fe II	2402.0807	P	2402.0964	-0.0157	2402.0951	-0.0144	2402.0771	0.0036
Fe II	2401.8949	P	2401.8947	0.0002	2401.8933	0.0016	2401.8749	0.0200
Fe II	2401.2918	H	2401.2942	-0.0024	2401.2924	-0.0006	2401.2731	0.0187
Fe II	2400.3443	H	2400.3429	0.0014	2400.3407	0.0036	2400.3205	0.0238
			2400.0470		2400.0447		2400.0244	
			2399.7954		2399.7929		2399.7726	

Table A.14: Wavelength table for order 14(198).

Ion	ID'd λ_{vac}		Ind. Fit λ_{vac}	$\Delta\ \lambda_{vac}$	3 Deg. λ_{vac}	$\Delta\ \lambda_{vac}$	Hybrid λ_{vac}	$\Delta\ \lambda_{vac}$
Fe II	2396.7197	P	2396.7231	-0.0034	2396.7210	-0.0013	2396.7204	-0.0007
	2396.5354	P	2396.5329	0.0025	2396.5308	0.0046	2396.5300	0.0054
Fe II	2396.1014	H	2396.1017	-0.0003	2396.0998	0.0016	2396.0982	0.0032
Fe II	2395.6254	H	2395.6247	0.0007	2395.6228	0.0026	2395.6204	0.0050
Fe II	2395.4193	H	2395.4196	-0.0003	2395.4179	0.0014	2395.4149	0.0044
?	2395.1975	P	2395.1940	0.0035	2395.1923	0.0052	2395.1888	0.0087
?	2393.8250	P	2393.8295	-0.0045	2393.8282	-0.0032	2393.8212	0.0038
			2393.3536		2393.3523		2393.3440	
			2393.1786		2393.1773		2393.1686	
			2392.5875		2392.5862		2392.5758	
Fe II	2391.9586	P	2391.9575	0.0011	2391.9561	0.0025	2391.9440	0.0146
			2391.4771		2391.4756		2391.4622	
			2390.9630		2390.9612		2390.9465	
Fe II	2390.7645	H	2390.7652	-0.0007	2390.7633	0.0012	2390.7481	0.0164
Fe II	2390.0971	H	2390.0963	0.0008	2390.0938	0.0033	2390.0772	0.0199
Fe II	2389.9730	H	2389.9730	0.0000	2389.9704	0.0026	2389.9535	0.0195
Fe II	2388.6289	H	2388.6291	-0.0002	2388.6246	0.0043	2388.6058	0.0231
?	2388.3740	P	2388.3726	0.0014	2388.3676	0.0064	2388.3486	0.0254
			2388.2393		2388.2341		2388.2150	

Table A.15: Wavelength table for order 15(199).

Ion	ID'd λ_{vac}		Ind. Fit λ_{vac}	$\Delta\ \lambda_{vac}$	3 Deg. λ_{vac}	$\Delta\ \lambda_{vac}$	Hybrid λ_{vac}	$\Delta\ \lambda_{vac}$
Fe II	2384.4231	H	2384.4234	-0.0003	2384.4139	0.0092	2384.4131	0.0100
Fe II	2383.2452	H	2383.2444	0.0008	2383.2370	0.0082	2383.2343	0.0109
Fe II	2381.8362	H	2381.8368	-0.0006	2381.8307	0.0055	2381.8248	0.0114
Fe II	2380.7616	H	2380.7617	-0.0001	2380.7563	0.0053	2380.7476	0.0140
			2380.5032		2380.4980		2380.4886	
			2380.2042		2380.1992		2380.1890	
			2379.8052		2379.8005		2379.7893	
Fe II	2379.2765	H	2379.2768	-0.0003	2379.2725	0.0040	2379.2601	0.0164
			2378.8196		2378.8159		2378.8024	
Fe II	2378.1171	H	2378.1163	0.0008	2378.1138	0.0033	2378.0988	0.0183
Fe II	2377.2274	P	2377.2278	-0.0004	2377.2275	-0.0001	2377.2110	0.0164
			2376.4199		2376.4224		2376.4050	

Table A.16: Wavelength table for order 16(200).

Ion	ID'd λ_{vac}		Ind. Fit λ_{vac}	$\Delta\ \lambda_{vac}$	3 Deg. λ_{vac}	$\Delta\ \lambda_{vac}$	Hybrid λ_{vac}	$\Delta\ \lambda_{vac}$
Fe I	2371.4305	H	2371.4306	-0.0001	2371.4248	0.0057	2371.4228	0.0077
Fe II	2369.9534	H	2369.9506	0.0028	2369.9437	0.0097	2369.9389	0.0145
Fe II	2369.7274	H	2369.7301	-0.0027	2369.7233	0.0041	2369.7180	0.0094
Fe I	2369.4563	H	2369.4571	-0.0008	2369.4503	0.0060	2369.4443	0.0120
Fe II	2368.5964	H	2368.5955	0.0009	2368.5889	0.0075	2368.5810	0.0154
?	2367.0411	P	2367.0394	0.0017	2367.0332	0.0079	2367.0218	0.0193
Fe II	2366.8880	P	2366.8843	0.0037	2366.8781	0.0099	2366.8664	0.0216
Fe II	2366.5938	H	2366.5937	0.0001	2366.5875	0.0063	2366.5752	0.0186
Fe II	2365.7654	H	2365.7656	-0.0002	2365.7590	0.0064	2365.7451	0.0203
Fe II	2363.8612	H	2363.8612	0.0000	2363.8511	0.0101	2363.8351	0.0261

Table A.17: Wavelength table for order 17(201).

Ion	ID'd λ_{vac}		Ind. Fit λ_{vac}	$\Delta\ \lambda_{vac}$	3 Deg. λ_{vac}	$\Delta\ \lambda_{vac}$	Hybrid λ_{vac}	$\Delta\ \lambda_{vac}$
Fe II	2361.0096	H	2361.0085	0.0011	2361.0075	0.0021	2361.0074	0.0022
Fe II	2360.5114	H	2360.5120	-0.0006	2360.5093	0.0021	2360.5089	0.0025
Fe II	2360.2945	H	2360.2935	0.0010	2360.2902	0.0043	2360.2896	0.0049
Fe II	2359.9997	H	2359.9990	0.0007	2359.9948	0.0049	2359.9939	0.0058
Fe II	2359.5958	H	2359.5955	0.0003	2359.5904	0.0054	2359.5890	0.0068
Fe II	2359.1072	H	2359.1140	-0.0068	2359.1079	-0.0007	2359.1058	0.0014
Fe II	2357.0488	H	2357.0405	0.0083	2357.0318	0.0170	2357.0260	0.0228
			2356.5912		2356.5822		2356.5755	
			2355.9037		2355.8946		2355.8865	
Fe II	2355.3504	H	2355.3524	-0.0020	2355.3432	0.0072	2355.3341	0.0163
			2355.2195		2355.2103		2355.2009	
			2355.0172		2355.0081		2354.9983	
Fe II	2354.8899	H	2354.8922	-0.0023	2354.8831	0.0068	2354.8731	0.0168
Fe II	2354.4778	H	2354.4784	-0.0006	2354.4694	0.0084	2354.4587	0.0191
Fe II	2353.6079	H	2353.6098	-0.0019	2353.6011	0.0068	2353.5890	0.0189
Fe II	2353.4699	H	2353.4676	0.0023	2353.4589	0.0110	2353.4466	0.0233
Fe II	2352.3093	H	2352.3087	0.0006	2352.3004	0.0089	2352.2869	0.0224

Table A.18: Wavelength table for order 18(202).

Ion	ID'd λ_{vac}		Ind. Fit λ_{vac}	$\Delta\ \lambda_{vac}$	3 Deg. λ_{vac}	$\Delta\ \lambda_{vac}$	Hybrid λ_{vac}	$\Delta\ \lambda_{vac}$
Fe II	2349.2692	H	2349.2690	0.0002	2349.2671	0.0021	2349.2671	0.0021
Fe II	2348.3025	H	2348.3028	-0.0003	2348.2985	0.0040	2348.2980	0.0045
Fe II	2348.1158	H	2348.1165	-0.0007	2348.1118	0.0040	2348.1112	0.0046
			2347.7756		2347.7704		2347.7695	
Fe II	2346.3544	H	2346.3528	0.0016	2346.3465	0.0079	2346.3439	0.0105
			2345.9356		2345.9293		2345.9260	
?	2345.5687	H	2345.5606	0.0081	2345.5542	0.0145	2345.5504	0.0183
Fe II	2345.3372	H	2345.3382	-0.0010	2345.3318	0.0054	2345.3276	0.0096
Fe II	2344.9845	H	2344.9967	-0.0122	2344.9903	-0.0058	2344.9856	-0.0011
Fe II	2344.6030	H	2344.6028	0.0002	2344.5964	0.0066	2344.5910	0.0120
Fe II	2344.2816	H	2344.2805	0.0011	2344.2741	0.0075	2344.2682	0.0134
Fe II	2344.1550	H	2344.1539	0.0011	2344.1474	0.0076	2344.1413	0.0137
Fe II	2343.9610	H	2343.9604	0.0006	2343.9539	0.0071	2343.9475	0.0135
Fe II	2343.4950	H	2343.4938	0.0012	2343.4871	0.0079	2343.4800	0.0150
Fe II	2343.3076	H	2343.3094	-0.0018	2343.3025	0.0051	2343.2951	0.0125
Fe II	2342.8882	H	2342.8857	0.0025	2342.8786	0.0096	2342.8705	0.0177
			2341.6482		2341.6393		2341.6295	
Fe II	2341.4525	P	2341.4515	0.0010	2341.4421	0.0104	2341.4320	0.0205
Fe II	2341.1749	H	2341.1755	-0.0006	2341.1654	0.0095	2341.1551	0.0198
Fe II	2340.4625	P	2340.4639	-0.0014	2340.4515	0.0110	2340.4405	0.0220

Table A.19: Wavelength table for order 19(203).

Ion	ID'd λ_{vac}		Ind. Fit λ_{vac}	Δ λ_{vac}	3 Deg. λ_{vac}	Δ λ_{vac}	Hybrid λ_{vac}	Δ λ_{vac}
Fe II	2336.8599	H	2336.8597	0.0002	2336.8242	0.0357	2336.8243	0.0356
Fe II	2334.7276	H	2334.7316	-0.0040	2334.7203	0.0073	2334.7191	0.0085
Fe II	2334.3212	H	2334.3156	0.0056	2334.3062	0.0150	2334.3045	0.0167
Fe II	2333.7084	H	2333.7099	-0.0015	2333.7020	0.0064	2333.6997	0.0087
Fe II	2333.2323	H	2333.2323	0.0000	2333.2249	0.0074	2333.2219	0.0104
Fe II	2332.7990	H	2332.7992	-0.0002	2332.7917	0.0073	2332.7882	0.0108
Fe II	2331.9747	H	2331.9748	-0.0001	2331.9665	0.0082	2331.9620	0.0127
Fe II	2329.9924	H	2329.9923	0.0001	2329.9831	0.0093	2329.9762	0.0162
			2329.3528		2329.3449		2329.3374	

Table A.20: Wavelength table for order 20(204).

Ion	ID'd λ_{vac}		Ind. Fit λ_{vac}	Δ λ_{vac}	3 Deg. λ_{vac}	Δ λ_{vac}	Hybrid λ_{vac}	Δ λ_{vac}
Fe II	2326.2212	H	2326.2198	0.0014	2326.2145	0.0067	2326.2148	0.0064
Fe II	2325.7149	H	2325.7171	-0.0022	2325.7140	0.0009	2325.7144	0.0005
Fe II	2325.2951	P	2325.2980	-0.0029	2325.2958	-0.0007	2325.2964	-0.0013
Fe II	2324.4731	H	2324.4720	0.0011	2324.4701	0.0030	2324.4707	0.0024
Fe II	2322.9412	H	2322.9487	-0.0075	2322.9439	-0.0027	2322.9440	-0.0028
Fe II	2322.4888	H	2322.4770	0.0118	2322.4711	0.0177	2322.4708	0.0180
Fe II	2321.7560	H	2321.7568	-0.0008	2321.7496	0.0064	2321.7488	0.0072
Fe II	2321.4928	H	2321.4979	-0.0051	2321.4904	0.0024	2321.4894	0.0034
Fe II	2321.2431	H	2321.2422	0.0009	2321.2345	0.0086	2321.2333	0.0098
Fe I	2320.3577	H	2320.3591	-0.0014	2320.3523	0.0054	2320.3503	0.0074
Fe II	2320.0348	H	2320.0330	0.0018	2320.0272	0.0076	2320.0249	0.0099
			2318.7558		2318.7583		2318.7548	
			2318.3090		2318.3164		2318.3126	
			2317.5681		2317.5865		2317.5819	
			2317.3177		2317.3406		2317.3358	

Table A.21: Wavelength table for order 21(205).

Ion	ID'd λ_{vac}		Ind. Fit λ_{vac}	Δ λ_{vac}	3 Deg. λ_{vac}	Δ λ_{vac}	Hybrid λ_{vac}	Δ λ_{vac}
?	2314.7023	H	2314.7031	-0.0008	2314.6974	0.0049	2314.6980	0.0043
?	2313.5641	H	2313.5621	0.0020	2313.5620	0.0021	2313.5632	0.0009
Fe II	2313.1041	H	2313.1000	0.0041	2313.1010	0.0031	2313.1024	0.0017
Fe II	2312.6117	H	2312.6155	-0.0038	2312.6170	-0.0053	2312.6186	-0.0069
Fe II	2312.3152	H	2312.3206	-0.0054	2312.3222	-0.0070	2312.3239	-0.0087
Ni I	2310.9618	H	2310.9558	0.0060	2310.9559	0.0059	2310.9576	0.0042
Fe II	2309.4438	H	2309.4476	-0.0038	2309.4444	-0.0006	2309.4456	-0.0018
Fe I	2308.9989	H	2308.9974	0.0015	2308.9932	0.0057	2308.9942	0.0047
Fe II	2306.6693	H	2306.6692	0.0001	2306.6637	0.0056	2306.6631	0.0062

Table A.22: Wavelength table for order 22(206).

Ion	ID'd λ_{vac}		Ind. Fit λ_{vac}	Δ λ_{vac}	3 Deg. λ_{vac}	Δ λ_{vac}	Hybrid λ_{vac}	Δ λ_{vac}
Fe I	2303.5806	H	2303.5812	-0.0006	2303.5831	-0.0025	2303.5837	-0.0031
Fe I	2303.4243	H	2303.4234	0.0009	2303.4253	-0.0010	2303.4261	-0.0018
Fe II	2301.1740	H	2301.1747	-0.0007	2301.1725	0.0015	2301.1753	-0.0013
Fe II	2300.5240	H	2300.5254	-0.0014	2300.5218	0.0022	2300.5251	-0.0011
Fe I	2300.1418	H	2300.1432	-0.0014	2300.1390	0.0028	2300.1426	-0.0008
Fe II	2299.7509	H	2299.7440	0.0069	2299.7394	0.0115	2299.7431	0.0078
Fe II	2299.2201	H	2299.2219	-0.0018	2299.2172	0.0029	2299.2212	-0.0011
Fe I	2298.6602	H	2298.6609	-0.0007	2298.6569	0.0033	2298.6610	-0.0008
Fe II	2298.4469	H	2298.4502	-0.0033	2298.4468	0.0001	2298.4509	-0.0040
Fe I	2298.1690	H	2298.1685	0.0005	2298.1659	0.0031	2298.1701	-0.0011
Fe II	2297.7872	H	2297.7853	0.0019	2297.7844	0.0028	2297.7885	-0.0013
Fe II	2296.8912	H	2296.8914	-0.0002	2296.8966	-0.0054	2296.9007	-0.0095

Table A.23: Wavelength table for order 23(207).

Ion	ID'd λ_{vac}		Ind. Fit λ_{vac}	Δ λ_{vac}	3 Deg. λ_{vac}	Δ λ_{vac}	Hybrid λ_{vac}	Δ λ_{vac}
Fe II	2292.5248	H	2292.5243	0.0005	2292.5300	-0.0052	2292.5307	-0.0059
Fe II	2291.9990	H	2292.0002	-0.0012	2292.0054	-0.0064	2292.0067	-0.0077
Fe I	2291.1199	H	2291.1188	0.0011	2291.1228	-0.0029	2291.1254	-0.0055
Fe II	2289.0308	H	2289.0323	-0.0015	2289.0338	-0.0030	2289.0391	-0.0083
Fe II	2288.6629	H	2288.6622	0.0007	2288.6631	-0.0002	2288.6690	-0.0061
Fe II	2288.3570	H	2288.3570	0.0000	2288.3577	-0.0007	2288.3638	-0.0068
Fe I	2287.6311	H	2287.6300	0.0011	2287.6298	0.0013	2287.6366	-0.0055
Fe II	2287.2496	H	2287.2492	0.0004	2287.2486	0.0010	2287.2557	-0.0061
Fe II	2287.0506	H	2287.0517	-0.0011	2287.0509	-0.0003	2287.0581	-0.0075
Fe III	2284.0856	H	2284.0856	0.0000	2284.0830	0.0026	2284.0901	-0.0045

Table A.24: Wavelength table for order 24(208).

Ion	ID'd λ_{vac}		Ind. Fit λ_{vac}	Δ λ_{vac}	3 Deg. λ_{vac}	Δ λ_{vac}	Hybrid λ_{vac}	Δ λ_{vac}
Fe I	2279.9369	H	2279.9305	0.0064	2279.9298	0.0071	2279.9333	0.0036
Fe II	2279.7130	H	2279.7201	-0.0071	2279.7184	-0.0054	2279.7223	-0.0093
Fe II	2277.6671	H	2277.6683	-0.0012	2277.6719	-0.0048	2277.6798	-0.0127
Cu II	2276.2588	H	2276.2508	0.0080	2276.2611	-0.0023	2276.2711	-0.0123
Fe I	2274.0908	H	2274.0971	-0.0063	2274.0892	0.0016	2274.1008	-0.0100
?	2273.6095	H	2273.6051	0.0044	2273.5842	0.0253	2273.5957	0.0138

Table A.25: Wavelength table for order 25(209).

Ion	ID'd λ_{vac}		Ind. Fit λ_{vac}	Δ λ_{vac}	3 Deg. λ_{vac}	Δ λ_{vac}	Hybrid λ_{vac}	Δ λ_{vac}
Fe I	2267.4695	H	2267.4696	-0.0001	2267.4749	-0.0054	2267.4828	-0.0133
Fe I	2267.0847	H	2267.0845	0.0002	2267.0892	-0.0045	2267.0982	-0.0135
Fe I	2266.9058	H	2266.9060	-0.0002	2266.9114	-0.0056	2266.9208	-0.0150
Fe I	2264.3893	H	2264.3893	0.0000	2264.3926	-0.0033	2264.4073	-0.0180
Ne	2263.1662	H	2263.1662	0.0000	2263.0867	0.0795	2263.1025	0.0637

Table A.26: Wavelength table for order 26(210).

Ion	ID'd λ_{vac}		Ind. Fit λ_{vac}	Δ λ_{vac}	3 Deg. λ_{vac}	Δ λ_{vac}	Hybrid λ_{vac}	Δ λ_{vac}
Fe I	2259.5103	H	n/a		2259.5208	-0.0105	2259.5220	-0.0117
Fe II	2257.0909	H	n/a		2257.1006	-0.0097	2257.1086	-0.0177
Fe II	2255.1411	H	n/a		2255.1492	-0.0081	2255.1635	-0.0224
Fe II	2251.8230	H	n/a		2251.8289	-0.0059	2251.8492	-0.0262

Table A.27: Wavelength table for order 27(211).

Ion	ID'd λ_{vac}		Ind. Fit λ_{vac}	Δ λ_{vac}	3 Deg. λ_{vac}	Δ λ_{vac}	Hybrid λ_{vac}	Δ λ_{vac}
Fe II	2249.1967	H	2249.1926	0.0041	2249.2055	-0.0088	2249.2059	-0.0092
Fe II	2249.0589	H	2249.0577	0.0012	2249.0709	-0.0120	2249.0715	-0.0126
Fe I	2248.8602	H	2248.8677	-0.0075	2248.8813	-0.0211	2248.8824	-0.0222
Fe II	2247.6840	H	2247.6818	0.0022	2247.6964	-0.0124	2247.7006	-0.0166
Fe II	2247.3381	H	2247.3350	0.0031	2247.3494	-0.0113	2247.3548	-0.0167
Fe II	2246.6487	H	2246.6535	-0.0048	2246.6672	-0.0185	2246.6750	-0.0263
Fe II	2245.4993	H	2245.4976	0.0017	2245.5093	-0.0100	2245.5217	-0.0224
Fe II	2244.9165	H	2244.9139	0.0026	2244.9244	-0.0079	2244.9392	-0.0227
Fe II	2244.2443	H	2244.2468	-0.0025	2244.2559	-0.0116	2244.2732	-0.0289
Fe II	2243.2649	H	2243.2649	0.0000	2243.2723	-0.0074	2243.2930	-0.0281
Fe II	2243.0817	H	2243.0821	-0.0004	2243.0893	-0.0076	2243.1106	-0.0289
Cu II	2242.6181	H	2242.6179	0.0002	2242.6247	-0.0066	2242.6472	-0.0291
Fe II	2241.8775	H	2241.8772	0.0003	2241.8838	-0.0063	2241.9078	-0.0303

Table A.28: Wavelength table for order 28(212).

Ion	ID'd λ_{vac}		Ind. Fit λ_{vac}	Δ λ_{vac}	3 Deg. λ_{vac}	Δ λ_{vac}	Hybrid λ_{vac}	Δ λ_{vac}
Fe II	2238.5675	H	2238.5673	0.0002	2238.5824	-0.0149	2238.5828	-0.0153
Fe II	2237.4437	H	2237.4443	-0.0006	2237.4559	-0.0122	2237.4590	-0.0153
Fe II	2235.6809	H	2235.6805	0.0004	2235.6896	-0.0087	2235.6998	-0.0189
Fe II	2234.8844	H	2234.8842	0.0002	2234.8930	-0.0086	2234.9069	-0.0225
Fe II	2233.9176	H	2233.9180	-0.0004	2233.9267	-0.0091	2233.9453	-0.0277
Cu II	2230.0900	H	2230.0900	0.0000	2230.0976	-0.0076	2230.1272	-0.0372

Table A.29: Wavelength table for order 29(213).

Ion	ID'd λ_{vac}		Ind. Fit λ_{vac}	Δ λ_{vac}	3 Deg. λ_{vac}	Δ λ_{vac}	Hybrid λ_{vac}	Δ λ_{vac}
Cu I	2227.7782	H	2227.7781	0.0001	2227.7880	-0.0098	2227.7887	-0.0105
?	2225.7124	H	2225.7128	-0.0004	2225.7161	-0.0037	2225.7242	-0.0118
Fe II	2223.4860	H	2223.4854	0.0006	2223.4951	-0.0091	2223.5153	-0.0293
			2221.8237		2221.8372		2221.8658	
Fe II	2220.3783	H	2220.3794	-0.0011	2220.3895	-0.0112	2220.4229	-0.0446
Fe II	2219.8939	H	2219.8931	0.0008	2219.8999	-0.0060	2219.9340	-0.0401

Table A.30: Wavelength table for order 30(214).

Ion	ID'd λ_{vac}		Ind. Fit λ_{vac}	Δ λ_{vac}	3 Deg. λ_{vac}	Δ λ_{vac}	Hybrid λ_{vac}	Δ λ_{vac}
?	2216.6690	H	2216.6690	0.0000	2216.6766	-0.0076	2216.6788	-0.0098
Fe II	2215.0754	H	2215.0759	-0.0005	2215.0897	-0.0143	2215.0992	-0.0238
Fe II	2214.5859	H	2214.5838	0.0021	2214.5971	-0.0112	2214.6094	-0.0235
Fe II	2214.0317	H	2214.0348	-0.0031	2214.0466	-0.0149	2214.0624	-0.0307
Fe II	2213.6532	H	2213.6517	0.0015	2213.6621	-0.0089	2213.6804	-0.0272
?	2210.2676	H	2210.2676	0.0000	2210.2729	-0.0053	2210.3097	-0.0421

Table A.31: Wavelength table for order 31(215).

Ion	ID'd λ_{vac}		Ind. Fit λ_{vac}	Δ λ_{vac}	3 Deg. λ_{vac}	Δ λ_{vac}	Hybrid λ_{vac}	Δ λ_{vac}
Fe II	2201.5864	H	n/a		2201.5894	-0.0030	2201.6214	-0.0350
Fe I	2200.7243	H	n/a		2200.7269	-0.0026	2200.7642	-0.0399
Fe I	2200.3900	H	n/a		2200.3778	0.0122	2200.4170	-0.0270
?	2199.5898	H	n/a		2199.5908	-0.0010	2199.6331	-0.0433

Table A.32: Wavelength table for order 32(216).

Ion	ID'd λ_{vac}		Ind. Fit λ_{vac}	Δ λ_{vac}	3 Deg. λ_{vac}	Δ λ_{vac}	Hybrid λ_{vac}	Δ λ_{vac}
Fe I	2196.0420	H	n/a		2196.0377	0.0043	2196.0391	0.0029
?	2192.2661	H	n/a		2192.2663	-0.0002	2192.2936	-0.0275
Fe I	2191.8391	H	n/a		2191.8358	0.0033	2191.8667	-0.0276
Fe I	2191.2043	H	n/a		2191.2006	0.0037	2191.2365	-0.0322

Table A.33: Wavelength table for order 33(217).

Ion	ID'd λ_{vac}		Ind. Fit λ_{vac}	Δ λ_{vac}	3 Deg. λ_{vac}	Δ λ_{vac}	Hybrid λ_{vac}	Δ λ_{vac}
Fe I	2186.8926	H	2186.8910	0.0016	2186.8712	0.0214	2186.8704	0.0222
Fe I	2186.4869	H	2186.4889	-0.0020	2186.4692	0.0177	2186.4685	0.0184
Ne III	2182.2633	H	2182.2627	0.0006	2182.2441	0.0192	2182.2718	-0.0085
?	2181.7371	H	2181.7356	0.0015	2181.7175	0.0196	2181.7501	-0.0130
?	2180.8633	H	2180.8651	-0.0018	2180.8481	0.0152	2180.8883	-0.0250
Cu II	2179.4109	H	2179.4118	-0.0009	2179.3976	0.0133	2179.4478	-0.0369
Fe II	2178.9533	H	2178.9522	0.0011	2178.9391	0.0142	2178.9915	-0.0382